Confinement effects on freezing and melting

2001 J. Phys.: Condens. Matter 13 R95

(http://iopscience.iop.org/0953-8984/13/11/201)

INSTITUTE OF PHYSICS PUBLISHING JOURNAL OF PHYSICS: CONDENSED MATTER

J. Phys.: Condens. Matter **13** (2001) R95–R133 www.iop.org/Journals/cm PII: S0953-8984(01)10273-0

TOPICAL REVIEW

Confinement effects on freezing and melting

Hugo K Christenson

Department of Physics and Astronomy, The University of Leeds, Leeds LS2 9JT, UK

E-mail: phy6hkc@phys-irc.novell.leeds.ac.uk

Received 13 December 2000, in final form 2 February 2001

Abstract

A review of experimental work on freezing and melting in confinement is presented. A range of systems, from metal oxide gels to porous glasses to novel nanoporous materials, is discussed. Features such as melting-point depression, hysteresis between freezing and melting, modifications to bulk solid structure and solid–solid transitions are reviewed for substances such as helium, organic fluids, water and metals. Recent work with well characterized assemblies of cylindrical pores like MCM-41 and graphitic microfibres with slit pores has suggested that the macroscopic picture of melting and freezing breaks down in pores of molecular dimensions. Applications of the surface force apparatus to the study of freezing and melting phenomena in confinement are discussed in some detail. This instrument is unique in allowing the study of conditions in a single pore, without the complications of pore blockage and connectivity effects. The results have confirmed the classical picture of melting-point depression in larger pores, and allowed the direct observation of capillary condensation of solid from vapour. Other results include the measurement of solvation forces across apparently fluid films below the bulk melting point and a solid-like response to shear of films above the bulk melting point. These somewhat contradictory findings highlight the difficulty of using bulk concepts to define the phase state of a substance confined to nanoscale pores.

Contents

1. Introduction

Experimental studies of melting and freezing in confinement have been carried out since the early part of the 20th century. There is a large volume of literature dealing with a generally observed melting-point depression in porous media, and the results have been compared with theoretical predictions and used to gain information on the pore size distribution of the medium. The topic is of considerable practical relevance to areas such as frost heave, weathering of rocks and various man-made materials, the properties of porous media, oil recovery, ceramics and materials science in general.

A number of recent developments has seen increased interest in the area from a fundamental point of view. In addition to well-characterized materials of uniform pore size such as Vycor glasses, novel structures with isolated cylindrical pores or slit-pores of widths in the range 1–5 nm are now available. The results of some experiments with these porous media have been interpreted as showing a melting-point elevation in very narrow pores, in stark contrast to the almost universally observed depression in larger pores. In other cases the transitions appear to be fundamentally different from those observed in bulk. One appears to be observing a change from three-dimensional to two- or even one-dimensional phase behaviour.

Experiments with the surface force apparatus (SFA) based on capillary condensation from vapour are now being used to probe the behaviour of fluids close to and below the bulk melting point in what is effectively a single pore, thus eliminating uncertainties due to pore-size distribution and blocking of porous networks. Measurements can be carried out as a function of both temperature and pore size in one and the same experiment. These investigations have yielded information on phase behaviour and fluid structure in wedge-shaped pores and in slit pores. In addition, the SFA has been used to study the dynamic behaviour of fluid films a few molecular diameters thick by shearing the confining surfaces against each other.

In this review I will first summarize experimental results with porous media and then describe single-pore work on capillary melting and freezing with the SFA. The apparent contradiction between the capillary-condensation results that show classical melting-point depression, and dynamic experiments suggesting solid-like behaviour above the bulk melting point T_m, will be discussed with reference to the work on fluids in novel porous materials. It is hoped that the work to be presented will illustrate the potential for further study of freezing and melting transitions in a single pore with the SFA, and how this can shed light on the phase behaviour in porous media.

2. Background

2.1. Capillary condensation

Capillary condensation of liquid from undersaturated vapour is a well-known phenomenon that has been extensively studied since it was first described by W Thomson (Lord Kelvin) [1]. In the common text-book derivation the Laplace equation describing the pressure difference across a curved liquid–vapour interface of surface tension γ_{lv} is used to show how undersaturated vapour of relative vapour pressure p/p_0 coexists with a liquid in a pore. If the contact angle θ of the liquid on the surface of the pores is less than 90° and the liquid–vapour interface consequently concave, the radius of curvature r of the liquid–vapour interface is negative and the classical Kelvin equation is

$$r = -\frac{\gamma_{lv} v_m}{kT \ln[p/p_0]} \tag{1}$$

where v_m is the molecular volume of the liquid.

Similarly, the increased vapour pressure over convex droplets (r positive) forms the basis of the classical theory of homogeneous nucleation from vapour, where it is shown that there is a minimum size below which a condensed droplet is unstable.

Alternatively, capillary condensation may be viewed as an effect of confinement on the vapour–liquid transition, whereby the wetting of the solid walls by the liquid in preference to the vapour phase causes condensation at a chemical potential off bulk coexistence [2, 3]. In this approach, the curvature of the interfaces is not directly treated, and the problem reduces to one of comparing the magnitudes of surface tension terms. For an infinite slit of width H (figure 1, top) the Kelvin equation gives

$$\frac{H}{2\cos\theta} = -\frac{v_m \gamma_{lv}}{kT \ln[p/p_0]}. \tag{2}$$

Using the Young equation

$$\gamma_{sv} = \gamma_{sl} + \gamma_{lv}\cos\theta. \tag{3}$$

where γ_{sv} is the surface tension of the solid–vapour interface and γ_{sl} is the surface tension of the solid–liquid interface, one obtains

$$H = -\frac{2v_m[\gamma_{sv} - \gamma_{sl}]}{kT \ln[p/p_0]}. \tag{4}$$

The relationships of equations (2) and (4) may also be derived directly using bulk and surface thermodynamic arguments, as shown in [3]. The equilibrium separation H thus depends directly on the relative magnitudes of the surface tension of the solid substrate in vapour and in liquid. This is in many ways a more convenient formulation of the problem as one does not consider explicitly the liquid–vapour interface, about which there is often no direct information. This treatment is thus similar to the classical nucleation problem in that one considers a balance of bulk and surface energy terms to establish stability criteria for vapour and condensed liquid.

2.2. Capillary melting

The possibility of an effect of confinement on the solid–liquid transition follows directly from the type of argument presented above. If the liquid wets the container walls in the presence of the solid phase the liquid will be thermodynamically favoured in confinement. Since pressure effects on a solid–liquid transition are small, the most obvious physical manifestation will be a reduced melting point. This corresponds most directly to the expectation of an elevated boiling point for the case of a confined liquid, i.e. capillary condensation above the bulk liquid–vapour transition.

In the older literature the melting-point depression is usually introduced as a consequence of the reduction in pressure over a concave liquid meniscus in a pore [4]. The reduction in equilibrium vapour pressure leads to a shift in the intersection of the equilibrium line between capillary-held liquid and vapour and the bulk solid–vapour line towards lower temperatures. Liquid in the pores is thus in equilibrium with bulk solid at a temperature below T_m. Note, however, that capillary-held solid may show a reduced or an enhanced vapour pressure, depending on the curvature of the solid–vapour interface (and hence the wetting properties of the solid in the pores). Depending on the signs and relative magnitudes of the shifts in vapour pressure over the confined solid and liquid, the equilibrium point of capillary solid and capillary liquid may be reduced or enhanced compared to T_m. The quantitative dependence of the melting- (freezing-) point depression ΔT ($= T_m - T_m(\text{pore})$) on the pore radius of the samples has been derived using the Clausius–Clapeyron equation to give the vapour pressure as a function of temperature and the Kelvin equation to correlate this vapour pressure with the pore radius. In this manner one obtains, for a cylindrical pore of radius r [4],

$$\Delta T = -\frac{T_m}{\Delta H_f}\frac{2}{r}[V_l\gamma_l - V_s\gamma_s] \tag{5}$$

where ΔH_f is the enthalpy of fusion (latent heat of melting), V_l and V_s the molar volumes of the liquid and solid, respectively, and γ_l and γ_s the corresponding surface energies, the temperature dependence of which is customarily neglected. With the assumption that the solid is wetted by its own melt (i.e. $\gamma_s - \gamma_l = \gamma_{sl}$) and if the change in molar volume at T_m is neglected, this simplifies to

$$\Delta T = \frac{2T_m V_m \gamma_{sl}}{r\Delta H_f}. \tag{6}$$

This relationship is generally known as the Gibbs–Thomson equation, both when used to describe melting in pores as well as melting of small particles (see 2.4). A thermodynamically rigorous treatment of melting in confinement via interfacial curvature becomes exceedingly complicated. In the full problem the vapour phase needs to be included and one has to contend with three interfaces, often of unknown or poorly defined curvature. The degree of confinement becomes a new set of phase variables that determines the thermodynamic state of the material, and the triple point is no longer fixed but depends on pore size. This has been discussed extensively by Defay *et al* [5] and others [6–8]. The problem is greatly simplified by considering a balance of bulk and surface free energy terms between solid and liquid, and it is this approach that has been most often used for melting in pores.

The free energy difference ΔG between liquid and solid in a pore at a temperature T can be expressed as

$$\Delta G = A[\gamma_{li} - \gamma_{si}] + V\Delta G_m \tag{7}$$

where ΔG_m is the free energy of fusion, γ_{li} is the substrate–liquid interfacial energy, γ_{si} is the substrate–solid interfacial energy, A is the total interfacial area between the material and

the substrate and V is the total volume of the confined material. The energies of any other interfaces in the system are ignored. ΔG_m is given by

$$\Delta G_m = \frac{[T_m - T]\Delta S_m}{V_m} = \frac{\Delta T \Delta H_f}{V_m T_m} \tag{8}$$

where ΔS_m is the entropy of melting, T is the melting point of the confined material, ΔH_f the heat of fusion and v_m the molar volume. This neglects the difference in molar volume and heat capacity between the solid and liquid. At equilibrium $\Delta G = 0$ and

$$\Delta T = \frac{A}{V}\frac{V_m T_m[\gamma_{si} - \gamma_{li}]}{\Delta H_f} \tag{9}$$

where A/V is geometry dependent. For a sphere of radius r, $A/V = 3/r$ and for a cylinder of radius r, $A/V = 2/r$, or in general $A/V = \alpha/r$

$$\Delta T = \frac{\alpha V_m T_m[\gamma_{si} - \gamma_{li}]}{r\Delta H_f} = \frac{\alpha V_m T_m \gamma_{sl}}{r\Delta H_f}. \tag{10}$$

The second equality in equation (10) follows if one assumes that the liquid will wet the solid material of the pore wall in the presence of the solid crystal. For most situations this would be a reasonable assumption, and this is in general borne out by the results of porous-media studies. Indeed, many models of freezing and melting in confinement assume the presence of non-freezing liquid layers between the confined solid and the pore walls. The situation is depicted schematically in figure 1. The middle sketch shows the case of a cylindrical solid plug and a spherical solid nucleus, both in contact with the walls in a pore of diameter d. The bottom shows the case when a liquid layer of thickness t persists near the pore walls, giving solid plugs or spheres of radius $r = (d-2t)/2$. For the case of a cylindrical pore, equation (10) is identical to equation (6), although the assumptions used in deriving the two equations are not exactly the same.

The above treatment of capillary melting is based on simple thermodynamics, without any reference to the molecular nature of the phases. Interactions between the container walls and the confined substance are taken care of by means of surface energy terms, and the relative magnitude of these compared to bulk terms determines the phase state of the material. Likewise, the Kelvin equation for capillary condensation does not explicitly consider adsorption of the vapour phase to the container walls and this only enters the problem indirectly through surface energy terms that modify the curvature of the interface.

The possible complications are much greater in the case of a liquid–solid transition than for a liquid–vapour transition. Even within the framework of a simple model one has to contend with variations in surface energy between different faces of a crystal, the possibility of different crystalline phases, amorphous or glassy states etc. At a higher level of sophistication, where interactions between the condensed phases and the substrate walls are treated more explicitly, further complications such as epitaxy, lattice mismatch, crystalline defects etc must be considered.

Whereas the Kelvin equation may be quite successfully corrected by allowing for the presence of an adsorbed layer at the vapour–substrate interface [2, 9] such a simple procedure is not readily available for the liquid–solid transition. The smaller the separation between the container walls, the more serious the consequences of neglecting the detailed structure of the solid–substrate interface will be. Wall effects on liquid structure may be said to decay over length scales of a few molecular diameters, whereas any perturbations in crystalline structure due to the substrate may be expected to be much longer range. Indeed, whereas wetting of a solid substrate by a liquid is a common occurrence there are few examples of wetting of a solid substrate by a crystal. The structure of a solid phase in confinement may be different from that in bulk at the same temperature, even for comparatively large pore diameters.

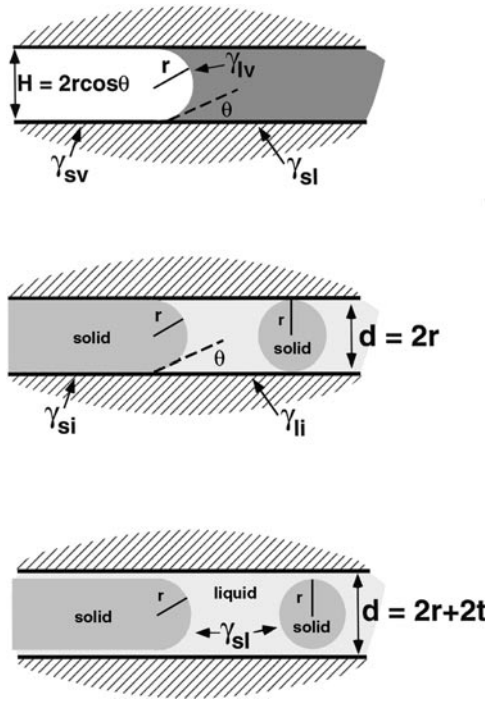

Figure 1. Top—schematic depiction of the equilibrium between vapour and liquid in a slit of width H. r is the radius of curvature of the liquid–vapour interface of energy γ_{lv} and radius of curvature r. θ is the contact angle of the liquid on the slit walls (substrate). γ_{sv} and γ_{sl} are the surface energies of the vapour–substrate interface and the liquid–substrate interface, respectively. Middle—solid–liquid transition in a cylindrical pore of diameter d. γ_{si} and γ_{li} are the surface energies of the solid–substrate interface and the liquid–substrate interfaces, respectively. θ is the contact angle of the liquid on the substrate in the presence of the solid phase, and r is the radius of the solid sphere or the solid, cylindrical plug. Bottom—as in middle sketch but with a non-freezing layer of thickness t on the substrate (pore wall).

Despite the complexity of behaviour noted above, much interpretation of experimental data has been based on simple models that allow for the existence of a non-freezing layer of liquid near the pore walls. This layer is typically one or two molecules thick, and its presence leads to an effectively reduced diameter of frozen material (as illustrated in figure 1, bottom). It also results in a reduced average enthalpy of melting in the pores and to an enhanced molecular mobility compared to bulk solid, and may contribute to the commonly encountered hysteresis between the freezing and melting temperatures.

2.3. Capillary freezing—hysteresis

A bulk first-order transition such as freezing almost always shows some degree of hysteresis and supercooling of impurity-free bulk liquids is the rule rather than the exception. In confinement the role played by heterogeneous nucleation at the pore walls becomes of paramount significance. While we may often expect heterogeneous nucleation of (wetting or near-wetting) liquid from vapour by pore walls, the same is not true for solid, whether nucleating directly from vapour or from the melt. The unfavourable solid–solid interfacial energies involved in the seeding of a crystal at a smooth and defect-free pore wall mean

that a kinetic model of freezing-point depression usually involves homogeneous nucleation in the centre of the pores. Freezing would only occur when the pore will accommodate the minimum-size stable solid nucleus, or for a cylindrical pore of radius r when

$$\Delta T = \frac{3V_m T_m \gamma_{sl}}{r \Delta H_f} \tag{11}$$

(see figure 1). The prediction of this kinetic model of freezing-point depression in a cylindrical pore thus differs by a factor of $3/2$ from that of the equilibrium model given by equation (10) with $\alpha = 2$, and the depression of the freezing point is expected to be greater than that of the melting point.

Melting of material in a cylindrical pore of radius r would still be expected to follow a relationship with $\alpha = 2$ in equation (10) and a prediction of hysteresis between freezing and melting is inherent in the kinetic model. The hysteresis between freezing and melting in porous media has been the subject of much discussion. Apart from nucleation effects the connection between hysteresis and pore geometry (ink-bottle effects etc), contact angle hysteresis, pore-size distribution, pore blockage on freezing etc have been considered. The nature of the equilibrium between liquid, solid and vapour has also been controversial—e.g. competition between freezing and sublimation.

2.4. Beyond melting and freezing

As long as the material in the pore can effectively be subdivided into surface and 'bulk' regions the treatment of the solid–liquid equilibrium is rather straightforward. As we have seen, the phase state is determined by a balance of the bulk term, related to the entropy of melting, and surface terms involving interactions with the pore walls and any vapour phase. Many of the results, particularly in the older literature, may be said to be probing this regime.

In the case of some of the more recent experiments with nanometre size pores it is obvious that no part of the confined material may be regarded as 'bulk'. Neither may the pore surface be assumed to be similar in structure and energy to that of a surface of bulk material in contact with a macroscopic wall. When the smallest dimension of the slits or cylinders is of the order of a few nanometres or less, there are no independent surfaces. The results in general point to a smearing of the transition between solid and liquid, and glassy-like states become important. Amorphous phases induced by confinement are frequently encountered even in porous systems with larger pores. Studies of substances showing glass transitions in bulk have demonstrated that the temperature depression of this transition induced by confinement is often significantly smaller than that of crystalline melting points, and there is a growing literature in this area [10].

The influence of confinement on freezing and melting phenomena is fundamentally a size effect, and as such is closely related to the study of melting of fine particles and thin films. In this case the first-order treatment also leads to a prediction of a lowered melting point for small particles due to the (in general) lower surface energy of the liquid compared to the solid. The topic is connected to surface melting, and the kinetics of the melting process are of crucial importance for establishing the correct definition of the melting point of a small particle. This review will not further consider small particles and the reader is referred to the literature [11–13]. Another related area is grain boundary melting in polycrystalline materials [14, 15], where unfavourable solid–solid interfacial contact also leads to the presence of liquid below the bulk melting point. The phase behaviour of systems of colloidal particles is another topic that falls outside the scope of this article [16, 17].

This article deals with experimental work, and for information on theory and simulation studies the reader is referred to the original literature [18–30] or to two recent reviews which have covered theoretical aspects of freezing and melting in confinement [31, 32].

3. Early studies of porous media

The first experiments on melting and freezing transitions in porous media reported evidence for the lack of a clear freezing transition at T_m, and for the existence of liquid far below this temperature. Information was obtained primarily from measurements of the vapour pressure as a function of temperature, and the break found at the melting point with bulk samples was seen to shift to lower temperatures. Similarly, dilatometry experiments revealed a temperature shift of the volume change associated with the liquid–solid transition. These investigations included dilatometry of water adsorbed on hydrogels like alumina, ferric oxide and silica [33, 34], vapour pressure measurements of benzene adsorbed on charcoal [35], dilatometry of water in egg white, silica gel and hydrated ferric oxide [36] as well as vapour pressure measurements of iodine on silica gel [37] and water on silica gel [38]. Studies were carried out with 1, 2-diaminoethane capillary condensed in 2.5 nm pore-size silica gel [39], and it was shown that dioxan adsorbed on ferric oxide gel ($r \sim 10$ nm) melts 6 °C below T_m, and that water on silica gel of $r \sim 1.1$ nm remains liquid at −65 °C [4]. The first calorimetric study [40] found a sizeable freezing-point depression for water, naphthalene, benzene and *p*-nitrotoluene adsorbed on silica gel. Later, the freezing-point lowering of benzene on charcoal and tetrachloromethane on silica gel was investigated calorimetrically, but only poor agreement between theory and experiment was obtained [41]. The freezing-point depression of water in silica gels, bentonite and clay loam was determined dilatometrically, and reasonable agreement between the measured freezing-point depression and theoretical predictions from vapour-pressure measurements and the Kelvin equation was found [42].

A calorimetric investigation of water and benzene adsorbed in silica gel with $d \sim 10$ nm also showed the absence of a melting transition at low coverage and an increasingly prominent heat-capacity peak that shifted progressively towards the bulk melting point with increasing coverage [43]. The authors concluded from the study that transfer of material from the adsorbed and capillary-condensed state to bulk crystals occurs via the vapour phase on cooling. NMR (nuclear magnetic resonance) studies of water in various silicas of wide pore-size distributions were interpreted in terms of a non-freezing layer of water adjacent to the pore walls [44]. Later NMR and dielectric measurements were also consistent with a layer of non-freezing water on the pore walls [45].

Much of this early literature discussed qualitatively observations and concepts that are still the subject of debate. Among these were the presence of strongly bound layers of molecules next to the pore walls, hysteresis between freezing and melting and the general broadening of the transitions, differences in the heat capacities of confined material compared to bulk and the effect of polydispersity of the pore size. In general, the poorly characterized materials available at the time precluded the accurate analysis of much of the data, and insufficient distinction was often made between melting and freezing.

4. Porous glasses

4.1. Early work

The availability of porous silicas with a range of reasonably monodisperse pore-size distributions has led to a tremendous increase in the amount of work on melting and freezing in confinement over the last 30–40 years. The transparency and amorphous nature of these materials mean that both optical studies and various scattering techniques may be employed to investigate the substances confined to the pores. Of further advantage is the relative ease with which the pore surface may be modified by adsorption or chemical modification, permitting

the control of wetting properties and contact angles. Vycor glass, formed by quenching (spinodal decomposition) and subsequent acid leaching of a SiO_2, B_2O_3 and Na_2O melt, has been the substrate of choice in these studies, and there is a large body of work concerned with characterization of Vycor glass [46–48]. Controlled-pore glasses (CPGs) are similar materials, and others are marketed under trade names like Spherisorb, Gasil etc. Sol–gel glasses are prepared in solution and then dehydrated at elevated temperatures to yield porous xerogels. A typical example of the pore geometry found in Vycor glass is shown in figure 2. As can be seen, the material consists of a network of essentially cylindrical pores, with varying degrees of connectivity.

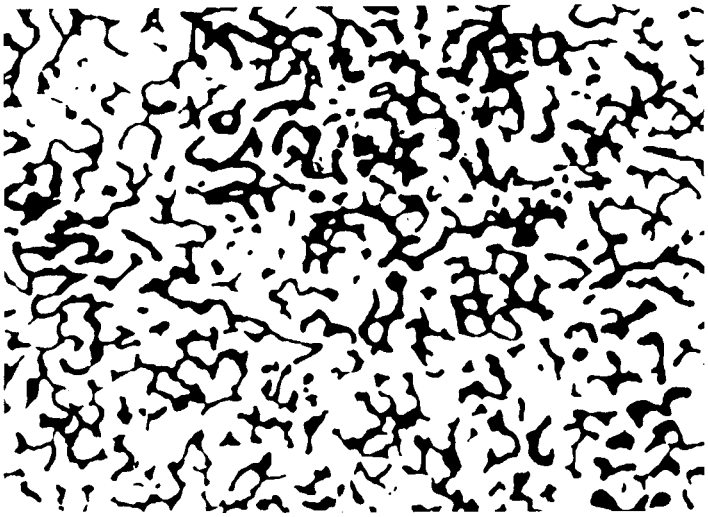

Figure 2. Digitized image of pore network in Vycor of mean pore diameter $d = 7$ nm, based on transmission electron micrographs of 30–40 nm thick sections. The porosity of the Vycor sample was 0.30 (from Levitz P, Ehret G, Sinha S K and Drake J M 1991 *J. Chem. Phys.* **95** 6151, used with permission).

One of the first studies using Vycor was a series of investigations of freezing phenomena with water, benzene and xenon [49–52]. Measurements of the expansion of the Vycor samples as a function of pressure at different temperatures were carried out with vapours of water and benzene. A gradual freezing process and a large hysteresis were found for both substances, and the authors discussed the influence of changing meniscus curvature in the pores between the liquid and solid state, and transport via a vapour phase [49, 50]. A subsequent study with water and xenon contained further discussion of the 'inadequacy of capillary condensation theory' [51]. Capillary-condensation theory refers to the assumption that the only difference between bulk material and the adsorbate is the lowered free energy due to the curved meniscus of the latter.

In a calorimetric study with water adsorbed to Vycor glass of mean pore diameter $d = 4.2$ nm no phase transition was found for low coverages, and at higher coverages the heat of fusion associated with the melting transition (at about $-10\,^{\circ}$C) was considerably smaller than in bulk [52]. The results were consistent with a bimolecular layer of non-freezing water adjacent to the pore walls.

In a study combining NMR relaxation measurements with DSC (differential scanning calorimetry) of water in silica samples with a range of pore sizes the picture of tightly bound water at the pore walls and 'bulk' water in the interior of the pores was given additional

support [53]. In this, one of the first such studies, the observed melting-point depression was inversely proportional to the pore radius, although the scatter was fairly large, and the smallest pores ($d \leqslant 5$ nm) showed deviations consistent with a non-freezing layer at the walls. Dilatometric and conductometric investigations of water in Vycor glass ($d \sim 7$ nm) gave a value for the ice-water interfacial energy of 29 mJ m^{-2} [54] using equation (6), close to other accepted estimates [55].

In what follows, studies of freezing and melting in porous glasses will be subdivided according to the substances investigated, starting with the quantum liquids helium and hydrogen, and moving on to inert gases, molecular gases, organic liquids, water and metals. Pore diameters will in general be quoted instead of radii, although there are cases were the original publication does not explicitly state which of the two is being used.

4.2. Hydrogen and helium

Work on the properties of liquid helium (mainly ^{4}He) in porous media as well as the search for a possible superfluid transition in molecular hydrogen [56, 57] led to widening interest among physicists in melting and freezing phenomena in confinement during the 1980s. Using specific heat measurements it was shown that helium confined to 6 nm pores in Vycor glass remained liquid well below temperatures at which bulk solid would form at elevated external pressure [58]. At the same time, the superfluid transition was observed to shift to lower temperatures (by about 0.25 K), with the result that superfluid would exist in the pores at temperatures and pressures which would lead to solidification in bulk [59]. Flow measurements in powder-packed tubes [60], and studies of the transverse sound velocity in ^{4}He confined to Vycor [61] confirmed these observations, and the interfacial energy between liquid and solid helium was estimated from the freezing temperatures using the nucleation model—equation (11) [61].

The complete phase diagram of helium in $d = 6$ nm Vycor was determined for pressures from 20 to 60 atm and temperatures between 1.2 and 2.3 K [62]—see figure 3. The latent heat on freezing of the normal liquid helium in the pores was found to be greater than in bulk, as expected since the bulk entropy is largely lost at the lambda transition. Ultrasonic attenuation and velocity studies of ^{4}He in Vycor ($d \sim 7$ nm) highlighted the role of vacancy diffusion in solid helium to maintain pressure equilibrium when the pores contained frozen helium [63]. Because of the high rate of diffusion in solid helium pore blockage is not a serious problem in freezing studies with this substance. Further work confirmed the expected inverse correlation between the pore diameter and the elevation of freezing-point pressure relative to bulk, as well as hysteretic effects [64, 65]. Calorimetric measurements of both ^{4}He [66] and ^{3}He [67] films in porous glasses focused on the superfluidity of such films.

The melting-point and freezing-point depressions as well as the specific heats associated with the transitions in 5.4 nm pores were determined in calorimetric studies of ^{4}He and D_2 in Vycor [68]. Further work established that in Vycor with pores of mean diameter less than 2.4 nm no freezing transition was observed for H_2 [69]. Hysteresis in the freezing and melting behaviour of the confined hydrogen was discussed in terms of the pore-size distribution and nucleation phenomena. No superfluid transition of liquid hydrogen in the smaller or in incompletely filled larger pores was detected down to 0.08 K, although with ^{4}He the transition was found to occur at 0.8 K [69]. The quest for superfluid hydrogen continues, and very recently superfluidity of very small assemblies of hydrogen appears to have been detected [70].

At temperatures above the bulk melting point at 18.7 K neutron diffraction measurements showed that the structure of D_2 in $d \sim 7$ nm pores was similar to that of the bulk liquid [72]. Between 14 and 15 K diffraction peaks appeared and were then relatively independent of temperature down to 4 K. On heating the peaks disappeared between 16 and 17 K, and the

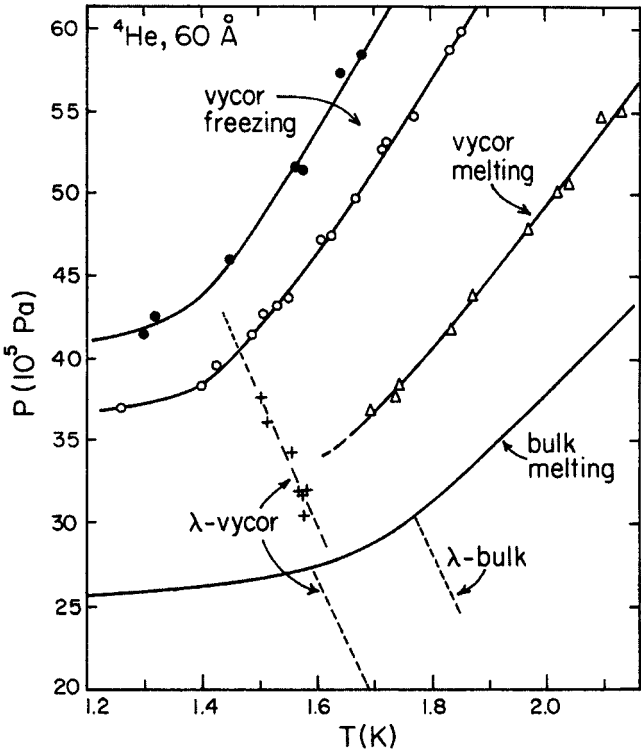

Figure 3. The phase diagram of ^{4}He in Vycor of $d = 6$ nm. Note the hysteresis between freezing and melting. Open circles show the onset of freezing, filled circles the completion of freezing and open triangles the completion of melting, all in Vycor (reproduced from Adams E D, Tang Y H, Uhlig K and Haas G E 1987 *J. Low Temp. Phys.* **66** 85, with kind permission of Kluwer Academic Publishers).

observed hysteresis between melting and freezing was in agreement with the earlier calorimetry results on H_2 [69]. The crystal structure of the crystalline deuterium was different from the bulk, and there was always an amorphous component (up to 80%) at all temperatures. The amorphous phase was attributed to unfrozen liquid or a glassy, solid-like phase such as might be present at the pore walls. In incompletely filled pores (filling fraction less than 0.5–0.6) no crystalline phase was found down to 4 K [71, 72]. The size of the frozen crystallites was much larger than the mean pore size, but their thermal expansion was identical to that of bulk material. Neutron-scattering experiments with H_2 [73] confirmed the behaviour found with D_2, with solidification to a crystalline structure unlike any found in bulk hydrogen, at a temperature of about 4 degrees below T_m.

In an investigation of hydrogen in Vycor with 6 nm diameter pores, using a torsional oscillator, vapour pressure data and capacitance measurements, it was found that an amorphous component adsorbed strongly to the pore walls. Excess hydrogen would leave the pores as the temperature was lowered [74, 75], in contrast to the results of a related study [73].

4.3. Inert gases

The freezing and melting of inert gases is not complicated by the occurrence of quantum effects as in the case of helium and possibly hydrogen. Moreover, the spherical symmetry of the atoms

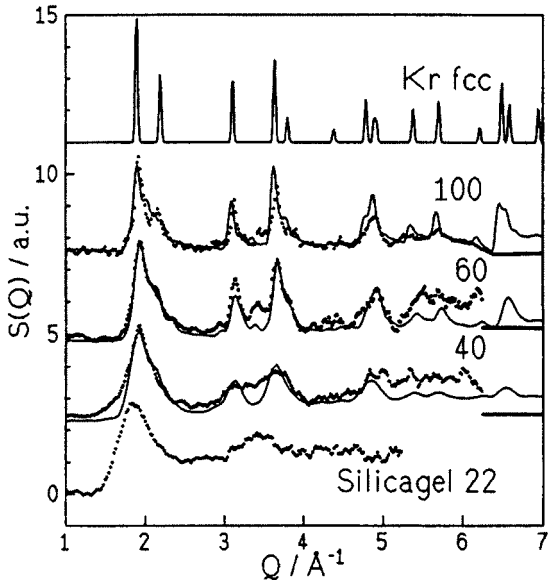

Figure 4. Difference x-ray diffraction patterns (dotted lines) of Kr in pores of silica gel of various mean pore diameters (in Å) at 40 K ($T_m = 119$ K), with the top curve denoting the reference—bulk fcc krypton. The solid lines are calculated diffractograms for Kr clusters of sizes similar to the pore diameters (from Schäfer B, Balszunat D, Langel W and Asmussen B 1996 *Mol. Phys.* **89** 1057 and http://www.tandf.co.uk, used with permission).

in the liquid state, and the fcc (face-centred cubic) structure of the bulk crystals mean that one is considering the simplest possible liquid–solid phase transition.

Calorimetric studies of neon in Vycor ($d = 5.4$ nm) found a depression in both freezing and melting temperatures, and from this a lower limit of the solid–liquid interfacial energy was calculated from the Gibbs–Thomson equation (equation (6)) to be 2.6 mJ m^{-2} [68]. As part of a larger study including oxygen (see below), hydrogen (referred to above) and neon, a detailed investigation of the freezing and melting hysteresis with argon in Vycor glass ($d = 7.2$ nm) was carried out [76]. Using ultrasonic attenuation and heat capacity measurements freezing was found to occur suddenly and rapidly below a certain temperature (8.4 K below T_m), independent of the cooling rate, but the total amount of liquid that would freeze increased as the temperature decreased. On subsequent warming, only a fraction of the frozen argon would remelt until a characteristic pore melting temperature ($\sim$3 K below T_m) was reached. By contrast, on renewed cooling the argon that had remelted would freeze immediately. The freezing process was thus irreversible, but melting appeared to be reversible.

These results were taken as an indication that pore geometry, and not kinetic factors such as nucleation rates, controlled freezing in the system. The dependence of total frozen amount on temperature would simply reflect the distribution of pore sizes, with the larger pores freezing first. Remelting would then occur at a higher temperature due to pore geometry (cylindrical pores, or necks between more spherical pores) or some rearrangement of amorphous layers on pore surfaces after freezing has occurred. The ratio between the observed freezing-point depression and melting-point depression was in fact close to the 3:2 predicted by theory—see equations (10) and (11).

Later work focused on the structure of solidified inert gases in porous media. X-ray powder diffraction of nanocrystals of krypton and xenon in silica gels with d ranging from 2.2 to 10 nm at temperatures far below T_m showed that the crystals had bulk structure, albeit with

stacking faults, in all but the smallest pores, where amorphous components dominated [77]—see figure 4. The coherence length of the crystallites was close to the pore diameter. An x-ray diffraction study of argon and krypton in Vycor ($d = 7$ nm) showed some differences between the structure of the confined crystals and bulk solid [78], and a solid–solid phase transition absent in bulk was identified. The freezing and melting points were depressed well below T_m, with the usual hysteresis. The diffraction results were consistent with the formation of a disordered hexagonal close-packed (dhcp) structure on freezing. The disorder was assumed to be due to a large number of stacking faults imposed by the proximity of the pore walls. At very low temperatures ($T \sim T_m/2$) the solid transformed to an fcc structure coexisting with a dhcp structure. The fcc structure appeared to propagate through considerable regions of the porous structure, with crystallite dimensions of the order of 100 nm, whereas the dhcp crystallites were comparable in size to the pore diameter. This transition to a more ordered structure on cooling was seen to be consistent with the expected greater importance of energy relative to entropy at low temperatures.

Using calorimetry and x-ray diffraction somewhat different results for argon were obtained with different porous glasses with d in the range 2.5–13 nm [79]. The low-temperature solid with a different crystalline structure was absent, and it was suggested that earlier results were due to insufficient equilibration. Instead, an fcc structure similar to the bulk crystal, albeit with numerous stacking faults, was found. It was argued that solid, crystalline argon is a thermodynamically stable 'solid capillary condensate' in analogy with liquid condensates found above and immediately below T_m. The possible occurrence of dewetting transitions in pores was discussed.

4.4. Nitrogen and oxygen

The diatomic molecules of oxygen and nitrogen adsorbed in porous glasses have been studied by several groups. Oxygen confined in sol–gel glass of pore diameters in the range 4.4–39 nm was studied by picosecond optical techniques [80, 81]. For coverages of less than about 2 monolayers (determined from adsorption isotherms) no phase transitions were evident, and there was no hysteresis between cooling and heating. At higher coverages a liquid–solid transition could be observed as an increase in scattered light, and the solid–solid transition corresponding to the bulk γ–β transition at 43.8 K showed up as a change in absorption. Both transitions were depressed compared to bulk, with a linear relationship between the depression of the freezing point and the inverse pore size—see figure 5. A small deviation for the largest pore size suggested genuine supercooling. The hysteresis between cooling and heating increased as the pore size diminished, but the freezing point was always well defined. The viscosity of liquid oxygen in the pores (as probed through measurements of the birefringence relaxation time) was identical to that of bulk oxygen at temperatures above T_m, but increased rapidly with decreasing temperatures below T_m. In connection with experiments with hydrogen, neon and argon (referred to above) oxygen was studied calorimetrically in $d = 7.2$ nm silica xerogel [76]. Depressed liquid–solid and solid–solid transitions, with hysteresis between freezing and melting, were confirmed.

A neutron diffraction study indicated that solid oxygen formed at a freezing-point depression of 5 K (similar to the above study) in 7 nm diameter pores (95% filled) had the bulk crystal structure of the γ phase, but that the crystallites were considerably larger—up to ten times—than the pores [71]. An amorphous component amounting to about 30% of the total scattering was found. Further neutron-diffraction investigations confirmed these observations, but failed to find any evidence of a crystalline solid in the smallest pores studied ($d = 3.5$ nm) [82]. The authors concluded that an amorphous solid phase with less order than in the liquid

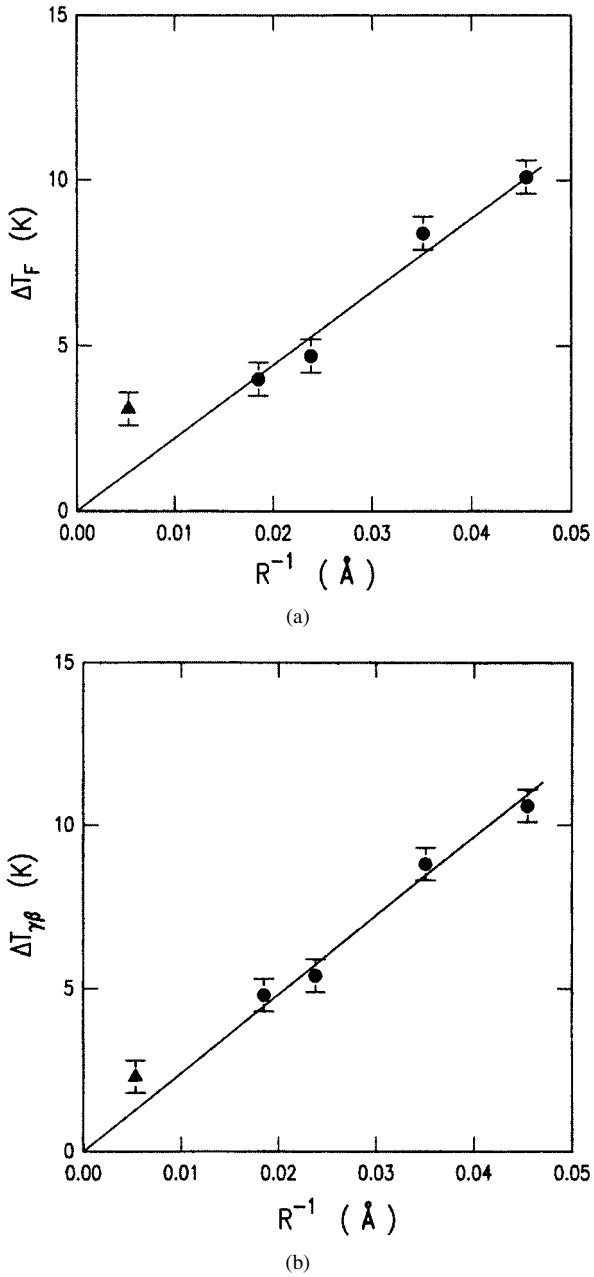

Figure 5. Observed depressions of the freezing point (a) and the γ–β solid transition (b) of oxygen in porous xerogel glass as a function of inverse pore radius. Note the slightly larger depression obtained for the largest pore size ($R = 18.8$ nm) (Awschalom D D and Warnock J 1987 *Phys. Rev.* B **35** 6779, copyright 1987 by the American Physical Society, used with permission).

above the solidification temperature formed in these pores, smaller than any in which oxygen had been previously studied.

An x-ray diffraction study of the structure of nitrogen in the pores ($d = 5$–7.5 nm) of a gelsil glass uncovered the expected freezing-point depression, but suggested that the bulk hcp

to fcc transition at 35 K was absent in the porous structure [83]. The structure of the frozen nitrogen was consistent with an amorphous component on the pore walls and an hcp crystal with a large number of stacking faults, as had been found with argon [79]. A comparative study of solid N_2 and CO in various porous glasses discussed differences in the structure compared to the bulk crystalline forms, and concluded that the solid condensates were always stable with respect to bulk solid [84]. There was no dewetting transition like that discussed for hydrogen [73–75] and argon [79].

4.5. Carbon dioxide

A systematic study of the phase diagram of carbon dioxide in 4 nm Vycor pores was carried out with positronium annihilation [85–88]. The lifetime and decay mode of positronium (electron–positron pairs), formed when positrons from a radioactive source enter the glass matrix, depend on the density of material in the pores. By monitoring the ratio of photons formed on decay of *ortho*-positronium to those formed by *para*-positronium one obtains a sensitive determinant of phase boundaries between vapour, liquid and solid. The results enabled the authors to map out the shift in phase boundaries, vapour–liquid, solid–liquid and solid–vapour, and consequently determine the triple point of carbon dioxide in 4 nm pores—see figure 6.

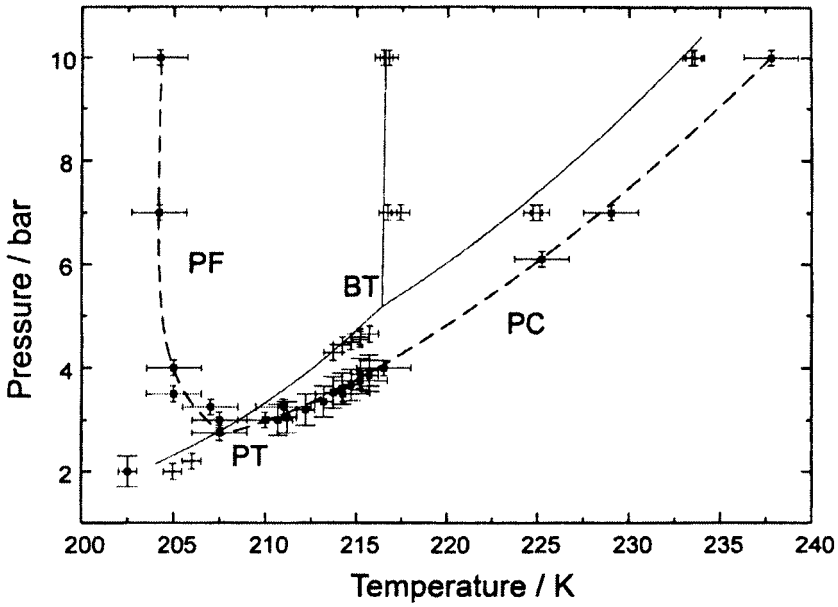

Figure 6. Phase diagram of CO_2 in Vycor glass of average pore diameter 4 nm, determined from positronium annihilation experiments. The solid line is the bulk phase diagram of CO_2, and the + symbols are phase transitions of bulk CO_2 obtained from positronium annihilation. The solid symbols with error bars are transitions on cooling at fixed pressure in the porous Vycor matrix. The dashed line PC shows the approximate loci of pore condensation transitions, PF the pore freezing transitions and PT the vapour–solid transitions in the pores, close to the corresponding bulk transition. BT is the bulk triple point, and PT the pore triple point (from Duffy J A, Wilkinson N J, Fretwell H M, Alam M A and Evans R 1995 *J. Phys.: Condens. Matter* **7** L713).

Related work discussed the hysteresis at the liquid–solid transition [89, 90], which was found to be similar to that discussed in detail for argon and other gases [76]. Pore blocking

was seen as a possible contributor, with a consequent reduction in pressure so that a complex melting process, proceeding perhaps via evaporation, would occur.

The structure of solid CO_2 in the pores was investigated by x-ray diffraction [91]. The confined solid was found to have the same structure as in bulk, albeit with slightly increased disorder. The dimensions of the crystallites were slightly larger than the mean pore diameter—16 nm versus 7 nm.

4.6. Methane

The dynamics of methane confined to various porous materials has been studied with inelastic neutron scattering. The results have shown that rotational disorder persists to very low temperatures (2–6 K) in silica gel ($d \sim 10$ nm) and there is no sign of crystallinity [92]. In controlled-pore glass of $d = 12$ and $d = 35$ nm there is coexistence of the ordered low-temperature bulk phase II with a disordered phase forming a 2 nm thick layer on the pore walls [93]. Similar phase coexistence occurs at a few degrees K in porous TiO_2 ($d \sim 11$ nm), and the melting is very broad, with a continuous increase in fraction of molecules in the liquid state, from 15 K below T_m at 91 K [94].

4.7. Organic liquids

Neutron diffraction, NMR and differential thermal analysis of cyclohexane in 9 nm pores of Spherisorb silica demonstrated depression of both T_m (279 K) and the transition from the plastic crystal (cubic) to the brittle crystal (monoclinic) at 186 K [95]. The mobility of the liquid molecules below T_m was reduced, but that of molecules in the plastic crystal enhanced, possibly due to the defective nature of the confined crystallites.

A comprehensive, calorimetric investigation of organic liquids in CPG glasses with pore diameters in the range 4–73 nm reported reductions in melting points and heats of fusion of the confined substances [96]. The studied liquids were *cis*-decalin, *trans*-decalin, cyclohexane, benzene, chlorobenzene, naphthalene and *n*-heptane, and the silica pores were hydrophobized with hexamethyldisilazane. From the melting-point depression, which was linear with inverse pore diameter—see figure 7, reasonable values of the solid–liquid interfacial energies were calculated, although the large spread in other available literature data made quantitative comparisons difficult. No sign of melting was observed for 4 nm pores in the case of cyclohexane and *cis*-decalin, suggesting that no freezing took place in these pores, possibly related to the disordered structure (i.e. plastic crystalline phases) of the bulk crystal. Furthermore, the enthalpies of fusion were also found to be strongly dependent on the pore diameters, with a substantial reduction compared to bulk in the smaller pores—see figure 8.

A detailed DSC study of cyclohexane in pores of Spherosil glass ($d = 4$–62.5 nm) showed depression of both the melting point and the monoclinic-to-cubic transition of the crystal [97]. The reduced heat of fusion was explained by postulating a linear change in enthalpy of fusion with pore area, due to non-participation in the phase transition by molecules adjacent to the pore walls.

A simple method to determine pore-size distribution using the proton NMR signal of cyclohexane was described [98]. The spin–spin relaxation time of the NMR signal is long for a liquid and short for a solid, and this can be used to find the proportion of unfrozen liquid as a function of temperature in a sample contained in a porous silica. The Gibbs–Thomson equation then yields the pore-size distribution, which was shown to agree well with results from gas desorption.

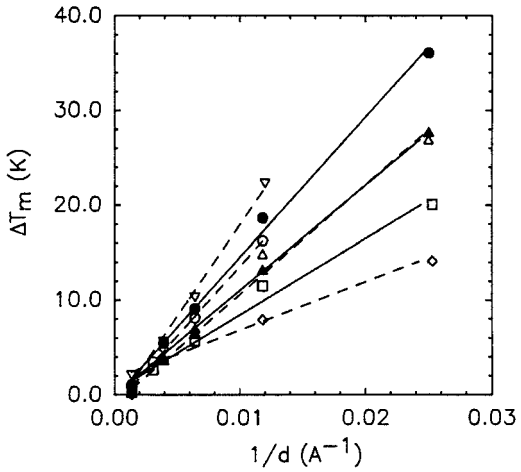

Figure 7. Experimental values of ΔT_m against $1/d$ from DSC (differential scanning calorimetry) of organic liquids in CPG glasses. The lines are linear regression fits used to calculate γ_{sl}. (○) *cis*-decalin, (●) *trans*-decalin, (▽) cyclohexane, (△) benzene, (▲) chlorobenzene, (◆) naphthalene and (□) *n*-heptane. Melting endotherms were not observed for cyclohexane and *cis*-decalin in the 40 Å pores (Jackson C L and McKenna G B 1990 *J. Chem. Phys.* **93** 9002, used with permission).

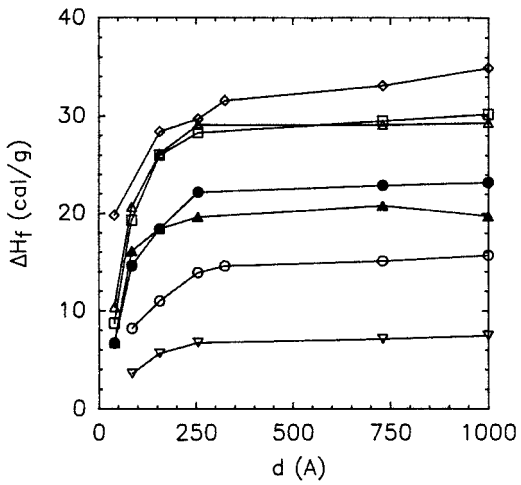

Figure 8. Values of ΔH_f as a function of pore diameter d from DSC of organic liquids in CPC glasses. Symbols as in the preceding figure. The bulk values are plotted for $d = 1000$ Å (Jackson C L and McKenna G B 1990 *J. Chem. Phys.* **93** 9002, used with permission).

In a related NMR study of porous silicas (Kiselgel of 4, 6, 10 and 20 nm diameter) the melting-point depressions of benzene and cyclohexane were compared with that of water [99]. The results could be fitted to a modified Gibbs–Thomson equation,

$$\Delta T = \frac{2T_m V_m \gamma_{sl}}{\Delta H_f} \frac{r}{r-t} \frac{1}{r} \tag{12}$$

where t represents the thickness of a layer of mobile (liquid-like) molecules next to the pore surface. When written in the above form, the reason for deviations from the $1/r$ proportionality for small r is emphasized. Alternatively, the results could be seen to reflect a molar heat

of fusion that decreases with pore diameter (i.e. ΔH_f becomes a function of r given by $\Delta H_f(\text{bulk})[r - t]/r$, where $\Delta H_f(\text{bulk})$ is the macroscopic heat of fusion in the limit of large r), in agreement with the results on a range of organic liquids in CPG glasses [96] discussed above.

Crystallization studies with cyclohexane in 6, 20 and 50 nm diameter Sorbsil silicas were also carried out with NMR [100]. The plastic crystalline phase was found to be absent in pores smaller than 5 nm (present because of a bimodal pore-size distribution in the nominally 6 nm pore-size samples), and was replaced with a structurally disordered phase with high rates of diffusion. In the 6 and 20 nm pores the cyclohexane was found to separate into two components at lower temperatures, and there were indications that a cubic phase became stable in the pores for low temperatures where the bulk structure is monoclinic. The bulk cubic–monoclinic transition was only seen in the 50 nm pores. Further NMR relaxation measurements of cyclohexane in silica gels showed that the dynamics at low temperatures was consistent with a liquid-like component at the pore surface and a plastic crystal in the centre of the pores [101].

2, 4, 6-trinitrotoluene (the explosive TNT) confined to porous gelsil glass of $d = 2.5$, 5, 10 and 20 nm was studied with DSC and temperature-dependent Raman scattering [102]. No freezing was observed in the smallest pores (2.5 and 5 nm), and the crystals in the larger pores had the bulk orthorhombic structure. Porous samples with excess bulk showed a much smaller freezing-point depression (the melting point was unaffected), which was interpreted to mean that the silica surface did not facilitate heterogeneous nucleation.

Succinonitrile solidifying and melting in a silica aerogel of a very wide pore-size distribution (r: 5–30 nm up to several μm) and open structure was studied with static light scattering [103]. Because of the open structure crystals would easily penetrate through the porous network and the observed hysteresis between freezing and melting was attributed to contact angle effects.

DSC studies of CCl_4 and nitrobenzene, and dielectric spectroscopy with nitrobenzene, in CPG and Vycor (d from 4–50 nm) showed a good linear correlation between the melting-point depression and the inverse pore radius [27]. The heat of fusion decreased with decreasing radius [27], although there was some deviation for nitrobenzene in the smallest pores. An equally good correlation and a reduced latent heat of melting emerged from a recent x-ray diffraction and DSC study of CCl_4 in silica gel of $d = 10$–100 nm [105]. A similar depression of the transition temperature and reduction in the enthalpy was found for the monoclinic to rhombohedral solid transition. On hydrophobic modification by reaction with hexadimethylsilazane no change in the phase transition temperatures was found. It was concluded that the reduction in the transition enthalpies was due to a non-freezing layer on the pore walls.

4.8. Water

Neutron diffraction experiments carried out on water confined to 9 nm diameter Spherisorb pores showed the presence of confined crystallites with a different structure to that of the bulk material [106, 107]. Cubic ice, previously only known from vapour deposition experiments or high-pressure studies, was shown to form when the pore water froze at $-13\,^{\circ}$C. An amorphous background component to the scattering was assumed to originate in the first few layers adjacent to the pore walls. In Gasil samples with a 2 nm pore diameter water remained liquid down to $-22\,^{\circ}$C. Later studies with sol–gel glasses of d in the range 4–50 nm showed a shift in the predominant ice species from hexagonal in the 50 nm pores to cubic in the 4 nm pores [108].

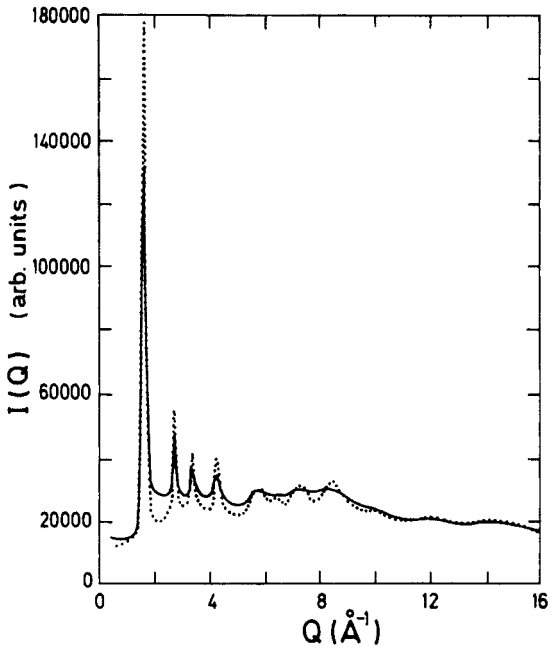

Figure 9. Neutron-scattering spectrum of D_2O confined to 5 nm (diameter?) Vycor at $-41.5\,^{\circ}C$ (solid line) and spectrum of bulk cubic ice at $-198\,^{\circ}C$ (dotted line). The spectrum of the D_2O in Vycor shows the presence of 27% liquid water (from Bellissent-Funel M-C, Lal J and Bosio L 1993 *J. Chem. Phys.* **98** 4246, used with permission).

NMR studies of water freezing in porous materials (silica gel, CPG and activated charcoal) showed a freezing-point depression consistent with two to three layers of non-freezing water on the pore surfaces [109].

In neutron scattering studies down to lower temperatures ($-100\,^{\circ}C$) [110] comparisons were made between fully and partially hydrated Vycor samples with 5 nm (diameter?) pores. The freezing-point depression determined calorimetrically agreed with the results of Rennie and Clifford [53], and was found to be greater in the partially hydrated Vycor. The structure of the confined ice was cubic (see figure 9), and liquid water was present down to $-40\,^{\circ}C$.

The usual hysteresis between freezing and melting was observed in NMR studies of water in porous Vycor glasses ($d = 3.6$–47 nm) [111], and from the melting-point depression as a function of pore radius a value of 27.5 mN m^{-1} for $\gamma_{ice-water}$ was calculated, consistent with other values in the literature. With increasing hydrophobicity of samples treated with hexamethyldisilazane the melting-point depression decreased, although no data could be obtained for the more hydrophobic samples due to the inability of water to penetrate the pores. This is consistent with a larger contact angle of the water–ice interface on the treated glass substrate, as was found experimentally.

A comprehensive study (by DSC, neutron diffraction, proton NMR relaxation and quasi-elastic light scattering) of thermal, structural and dynamic properties of water in the 3 and 10 nm diameter pores of Develosil glasses showed that water in the larger pores freezes to cubic ice, whereas no crystalline ice is formed in the smaller pores [112]. The authors discussed the influence of surface silanol groups on the dynamics of the confined water. Other studies with quasi-elastic and inelastic neutron scattering have concentrated on the dynamics of confined water below T_m [113–115]. Applications of neutron scattering techniques to the

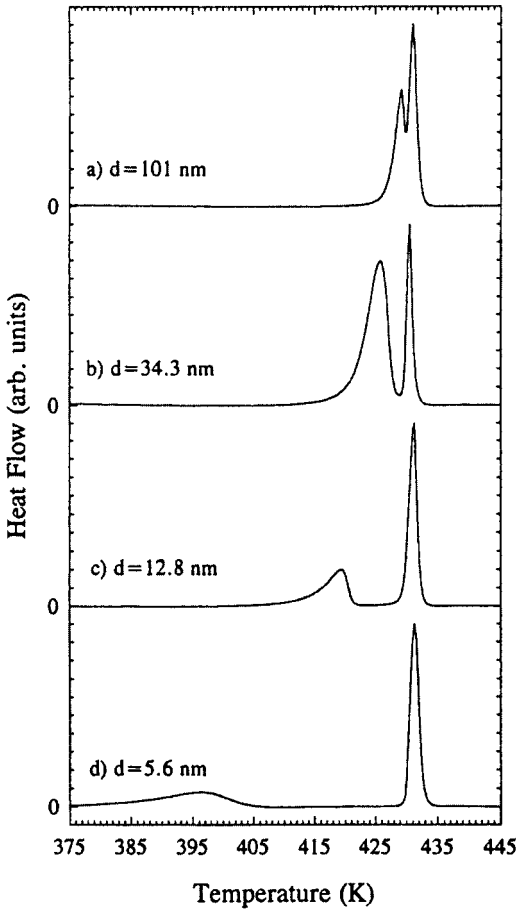

Figure 10. DSC melting scans for indium in CPG (a)–(c) and Vycor (d) glasses of varying pore diameters. Note the shift towards lower T and broadening of left-hand peak with decreasing d. The right-hand peak is the bulk melting peak of In (from Unruh K M, Huber T E and Huber C A 1993 *Phys. Rev.* B **48** 9021, copyright 1993 by the American Physical Society, used with permission).

characterization of porous materials and of confined substances have been dealt with in a recent review article [116].

4.9. Metals

In one of the first studies of melting and freezing of a metal in a porous medium a DSC investigation of indium in 6–141 nm pores of various Vycor and CPG was carried out [117]—see figure 10. The melting-point depression was proportional to $1/d$, and depending on assumptions regarding the pore geometry values of the solid–liquid interfacial energy in the range 21–64 mJ m^{-2} were obtained. The latent heat was size dependent, decreasing with decreasing pore size down to a value of one-third of the bulk value in the smallest pores. The crystal structure of solid indium in the Vycor pores as determined by x-ray diffraction was consistent with the bulk tetragonal structure, and the crystallite size was larger than the mean pore size. The deviation of the latent heat from the bulk value was taken to indicate a possible reduced latent heat for indium close to the pore walls.

The freezing and melting of mercury in Vycor ($d = 7$ nm) was studied by neutron diffraction, calorimetry, NMR and acoustical techniques [118–120]. As in the case of many previously mentioned wetting simple fluids, a depression of the freezing and melting points was found with this non-wetting system. Despite evidence that the size of the solid clusters (of the trigonal structure of bulk mercury) was temperature independent and equal to the pore diameter, there was considerable hysteresis, probably due to the non-wetting of the pore walls by the mercury. In other words, an evolution from spherical to cylindrical frozen particles could not explain the hysteresis. Rather, it was suggested that liquid-like skins on the solid particles near the pore walls gave rise to reversible freezing–melting behaviour, whereas the solid cores caused irreversibility.

Gallium in different porous glasses was studied in a series of experiments using electrical resistance measurements, x-ray diffraction, NMR and acoustical techniques [120–123]. Features discussed included the relative importance of freezing-point and melting-point depressions and the origin of the hysteresis based on geometrical changes. The structure of confined gallium was found to be different from the bulk structure and the size of the crystallites was larger than the pore diameter.

4.10. Summary of observations with porous glasses

The studies referred to above have largely confirmed the melting-point depression expected from the Gibbs–Thomson equation. There appears to be no clear exception to this behaviour among the vast range of substances investigated. Quantitatively, however, the observations differ and deviations are often observed for the smallest pore sizes. The enthalpy of fusion associated with melting in confinement has in general been found to be reduced compared to bulk [52, 96, 97, 99, 104, 105, 117] and the smaller the pores the greater the reduction. In almost all cases a temperature depression of any bulk solid–solid transition has also been observed, often of comparable magnitude to that of the melting transition.

The results of fits to the Gibbs–Thomson equation, as well as calorimetry scans and various diffraction measurements are by and large consistent with the presence of a non-freezing, or amorphous layer on the pore walls, typically some two molecular layers thick. This also strongly supports the contention that the solid almost never wets the pore walls.

The structure of the solid phases formed when liquid does freeze in porous glasses is often observed to deviate from the thermodynamically stable bulk structure [73, 106–108, 110]. The smaller the pores, the greater the difference from bulk. The structure may be a more disordered form of the bulk [91], or one with a greater number of lattice faults [77, 79, 83]. In some cases, notably that of water, the confined solid has a completely different crystalline structure [106–108, 110], and the likelihood of deviation from the bulk structure is greater the smaller the ratio between the pore size and the molecular diameter. The formation of amorphous solid may replace crystallization in the smallest pores [69, 82, 112], and often also in incompletely filled pores. Incompletely filled pores may show complete lack of a detectable transition [80, 81, 96, 102]. The solid crystallites are often seen to extend throughout sizable portions of the porous network, with the mean crystallite diameter many times the pore size.

Little work has been done on the effects of wetting of the pore walls by the liquid, but observations with water suggest that decreased wettability of the pore walls leads to a smaller depression of the freezing point. This may be viewed as an effect on the surface energy terms, and would render the assumption that liquid wets the substrate in the presence of solid invalid.

The question of the stability of confined solid relative to bulk has been the subject of some debate, with some evidence that condensed solid may leave the pores in favour of migration to a bulk reservoir [73–75, 79, 84]. This problem is tied in with the almost universally observed

hysteresis between melting and freezing, perhaps the least well understood feature of these experiments. In general, the extent of hysteresis appears to decrease with decreasing pore size, and the factors involved may include network effects [76] such as pore blockage and ink-bottle effects, solid–liquid equilibria involving confined vapour [89, 90], contact angle hysteresis [103], genuine supercooling as in bulk [80, 81] etc.

5. Porous silicon

Porous silicon is obtained by electrochemical etching of crystalline silicon wafers in hydrofluoric acid [124]. The microstructure of the pores depends on the level and type (n or p) doping of the silicon—the structure is either a random network of pores or a series of largely isolated but branching channels. In a recent DSC investigation of porous silicon with two kinds of pore structure—spherical with $d \sim 3$ nm and cylindrical with $d \sim 8$ nm—water, cyclohexane and *n*-dodecane were studied [125]. A larger hysteresis between freezing and melting was found for the cylindrical pores, and the results were consistent with the presence of a 1 nm non-freezing layer on the pore walls for *n*-dodecane, and a thicker, 1.7 nm layer for water.

6. Cylindrical pores—MCM-41 etc

MCM-41 (mobil catalyst material) is a novel substance consisting of a regular array of uniform, cylindrical pores with little or no interconnection [126, 127]. It is synthesized by hydrothermal reaction of aluminosilicate gels in the presence of quaternary ammonium surfactants. The diameter can be tailored in the range 1.6–10 nm according to preparation conditions. Several other, similar materials are available, and their synthesis has been described in the literature [128, 129].

An early study, using adsorption isotherm measurements and neutron diffraction, of a range of small molecules (N_2, CO, D_2, CH_4, Ar and Kr) adsorbed in MCM-41 ($d \sim 2.5$ nm) suggested that the structure of the confined material was either an amorphous solid or a fluid [130]. The freezing-point depression of water in MCM-41of $d \sim 4$ nm studied with NMR techniques showed good agreement with the Gibbs–Thomson equation when a non-freezing water layer of 0.35 nm was incorporated [131–133]. Very little hysteresis between freezing and melting, which occurred at about 230 K, was observed. The NMR technique was also used to investigate the pore-size distribution of the material [133].

Neutron diffraction of water at low temperatures (down to $-100\,^{\circ}$C) in MCM-41 with $d = 3.3$ and 3.5 nm indicated a structure incompatible either with cubic or hexagonal ice [108]. X-ray diffraction of water in MCM-41 with $d = 2.4$ and 4.2 nm confirmed the small or negligible freezing–melting hysteresis, and showed that water in the middle of the 4.2 nm pores froze abruptly at 232 K to yield cubic ice [134]. Freezing was more gradual in the 2.4 nm pores. In both cases, the results were consistent with the presence of a layer of disordered water next to the pore walls below the freezing point. In view of the lack of hysteresis found with these disconnected pores such a phenomenon in other mesoporous materials was attributed to a network effect. Support for this contention was provided by studies of the temperature dependence of the adsorption isotherms of Ar, N_2, O_2, C_2H_4, and CO_2 above T_m [135].

Further investigations to clarify the origin of these hysteresis effects were performed with water and a series of MCM-41 samples of pore diameters from 2.4 to 5.8 nm, and Vycor glass with $d = 7.2$ nm [136]. The hysteresis was found to be negligibly small in the pores of $d \leqslant 4.2$ nm, and then increased with increasing pore diameter, both for the MCM-41 and the Vycor samples. The melting point depression showed a linear relationship with the inverse

pore diameter for all samples, on the assumption of a bimolecularly thick layer of non-freezing water next to the pore walls. For $d \leqslant 3.5$ nm the freezing was not sharp, in contrast to the results with the larger pores, and it was suggested that a continuous transition to a disordered solid took place on freezing in the smaller pores.

Methane in MCM-41 was studied by neutron scattering and here a marked smearing of both melting and boiling was observed, with the existence of a regime of liquid-like methane extending to 30 K below the bulk m.p. and to 10 K above the bulk b.p. [137]. The onset of rotational melting (crystal to plastic crystal transition) was observed to differ from bulk, but shifted to higher temperatures.

Chloromethane confined to 2.4–5.8 nm pores studied by x-ray diffraction again showed large hysteresis effects for the larger pores ($d \geqslant 3.6$ nm) and vitrification in the smaller pores [138]. For $d \geqslant 5$ nm the solid structure is the same as in bulk, for $4.2 \geqslant d \geqslant 3.6$ nm the structure is different from bulk, whereas a glassy solid is formed for $d \leqslant 2.9$ nm. For $d \leqslant 4.2$ nm the freezing-point depression deviates significantly from an inverse pore radius correlation.

A series of liquids (water, cyclohexane, benzene, toluene, *o*-terphenyl and *m*-toluidine) was studied by DSC in pores of $d = 4$ nm [139]. Only slight melting-point depressions (a few K) compared to bulk were observed for cyclohexane, toluene and benzene, perhaps due to overfilling of the pores and freezing initiated by bulk material outside the pores. Water showed a larger depression, for reasons that were not discussed. The glass transition temperature for toluene, *o*-terphenyl and *m*-toluidine was hardly affected, being different from bulk only by less than one degree. Subsequently, however, NMR studies of benzene in MCM-41 ($d = 3$ nm) showed no sign of a phase transition in the range 148–298 K [140]. The molecular mobility decreased smoothly with temperature, as shown by the proton signal linewidth as a function of temperature (figure 11).

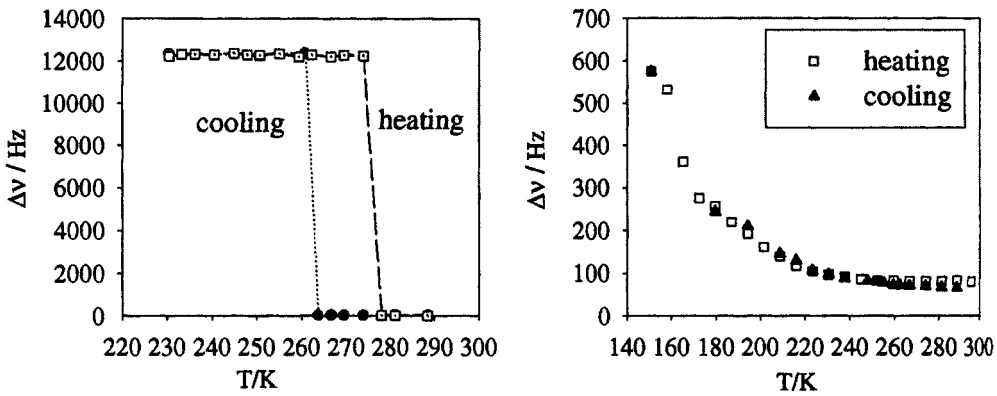

Figure 11. Proton NMR linewidth as a function of temperature for bulk benzene (left) and benzene confined to $d = 3$ nm MCM-41 (right). Note the continuous decrease with temperature for the confined benzene, and the absence of hysteresis (from Dosseh G, Morineau D and Alba-Simionesco C 2000 *J. Physique.* IV **10** Pr7-99, used with permission).

X-ray diffraction studies of nitrogen, CO and Kr in MCM-41 (d from 2.9 to 5.8 nm) showed further examples of vitrification in the narrowest pores (Kr in 2.9 nm, and CO and nitrogen in 4.2 nm), and crystallization in the larger pores, with a mixture of crystallization and vitrification in the intermediate-size pores [141]. Freezing and melting was almost reversible for all MCM-41 samples, and the freezing-point depression was approximately linear with inverse pore radius for all fluids. A subsequent study with Kr considered in more detail factors such as pore blockage, the capillary triple point and hysteresis [142].

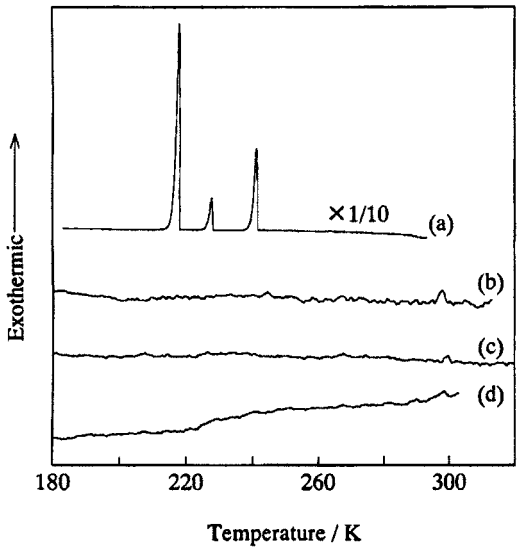

Figure 12. DSC cooling curves of bulk CCl_4 (a) and of CCl_4 in micropores of activated carbon fibres (ACFs) of varying slit widths: 1.13 nm (b), 0.82 nm (c) and 0.75 nm (d). (a) Shows the scan for bulk CCl_4 with the freezing peak at 240 K and two solid–solid transitions. Note the reduced scale for (a) (reprinted with permission from 1999 *J. Phys. Chem.* B **103** 7061, copyright 1999 American Chemical Society).

Similar studies of methanol in MCM-41 (d from 2.4 to 5 nm) and SBA-15 (7.8–14 nm) showed a progression from vitrification in the smaller pores (7.8 nm and smaller) to crystallization [143, 144]. A very large hysteresis between freezing and melting was observed in the larger pores, and depression of both transitions was large compared to that of water. The glass transition temperature in the smaller pores was independent of pore diameter.

7. Slit pores—graphitic microfibres

Activated carbon fibres prepared by pyrolysis and subsequent activation, usually with steam or CO_2, of fibres from coal-tar pitch [145] have recently been used in a number of fundamental studies of adsorption. Details of the manufacturing process are proprietary information, but the finished product consists of parallel lamellae of a graphitic structure, with most of the pore space in the material being slit shaped [146]. The slit width commonly varies between 0.7 and 2 nm, depending on preparation conditions.

X-ray diffraction of water in such slitlike ($d = 0.75$ and 1.13 nm) micropores of activated carbon showed considerable ordering over the range 143–303 K, with no clear phase transition point [147]. The structure in the wider pores was similar to that of bulk hexagonal ice, although the molecular mobility was higher than in bulk ice. The structure was more ordered in the 0.75 nm pores, and the mobility low, even at 303 K.

Studies of tetrachloromethane in similar pores also showed enhanced ordering and restricted mobility compared to that in bulk liquid at 303 K [148]. Differential scanning calorimetry of CCl_4 in pores of d from 0.75 to 1.13 nm over the range 180–320 K demonstrated a remarkable difference from bulk behaviour [149]. Both low-temperature solid–solid transitions were absent, and the only peak occurred at around 300 K, approximately 57 K above the bulk melting point. From its area the latent heat at this transition was found to be only

about 1% of the bulk enthalpy of freezing, and decreased with decreasing slit width (see figure 12).

For benzene in samples of similar slit width a single, diffuse DSC peak was found at a temperature of 16–20 K above the bulk melting point, and the latent heat was less than 0.1% of the bulk value [150]. X-ray diffraction studies of ethanol showed solid-like ordering and density at 303 K (well above the bulk melting point of 156 K) in pores of $d = 0.66$–1.13 nm [151].

8. Single pores

There are few accounts in the literature of experimental determinations of the melting-point depression in a single pore. An early attempt was made by Meissner in 1920 [152]. He found measurable decreases in the melting point of some organic substances confined to the wedge formed between a flat metal bar and a cylindrical glass lens. From the data he calculated values of the interfacial energy between solid and liquid, and found 50 mJ m^{-2} for tristearin, 59 for myristic acid and 67 for azobenzene. A similar method was subsequently used to study long-chain fatty acids in the wedge between a glass flat and a steel slab [153]. Further modifications involved the use of a glass cone formed by drawing out a Pyrex tube [154]. The results were used to determine the solid–liquid interfacial energy of ice, benzene, myristic acid and stearic acid. Later, more refined experiments gave what appeared to be an accurate and reproducible value of 21.7 ± 2 mJ m^{-2} for benzene [155]. This simple method of determining solid–liquid interfacial energies has not been widely used, and reasons for this were discussed in a review article [55].

With the surface force apparatus it is now possible to carry out accurate studies of melting and freezing behaviour both in a single, wedgelike pore and in thin films between curved or flat surfaces. This technique and some recent experiments are described in the next section.

9. The surface force apparatus

9.1. Introduction

The surface force apparatus [156–158] has been used extensively over the past 25 years to measure directly the force as a function of separation between surfaces in liquids and vapours. The two curved surfaces (usually of mica) are mounted in a crossed-cylinder configuration, and if one of these is mounted on a mechanical spring, its deflection allows the force between the surfaces to be determined. The surface separation is varied through use of a piezoelectric cylinder on which the second surface is rigidly held, and independently measured with multiple-beam interferometry [159]. White light is passed through the back-silvered mica surfaces and the wavelengths of the discrete fringes that are transmitted give the surface separation to an optimum accuracy of about 0.1 nm.

If the force-measuring spring is replaced with a mechanically more rigid support the two opposing surfaces become an ideal model pore for the study of confinement effects on phase behaviour (see figure 13) [160]. The surface separation can be controlled with greater precision as there is usually no spring deflection (except in the presence of very large force gradients). The interferometric technique used to measure the separation between the surfaces also permits the determination of the refractive index of material confined between the surfaces, which allows the phase state of this material to be identified. Supplementary information is provided by readily observable properties of the confined material such as its flow behaviour, its effect on the adhesion between the surfaces and its reaction to increasing or decreasing load (pressure)

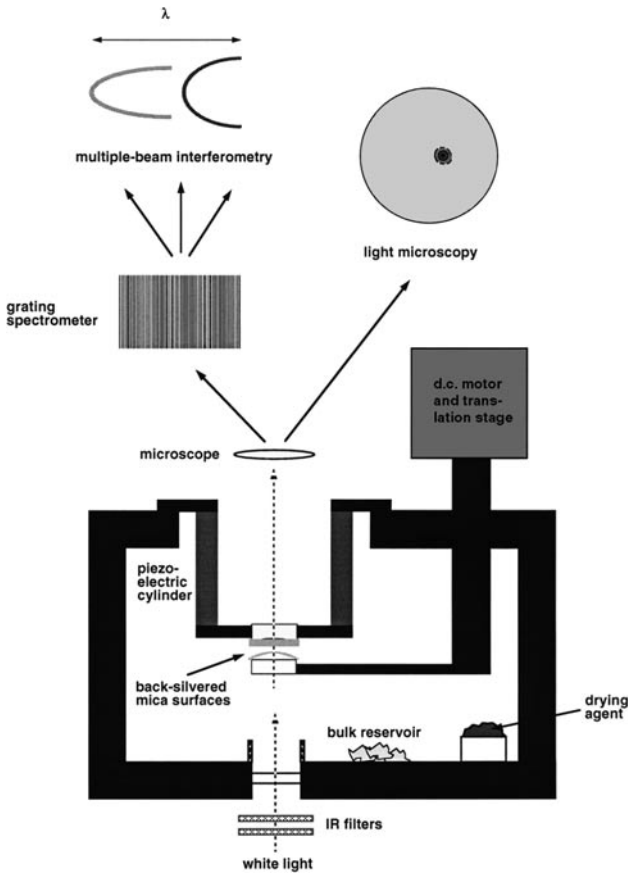

Figure 13. Schematic diagram of surface force apparatus (SFA) used for capillary-condensation studies of freezing and melting in confinement. For description see text.

on the confining surfaces. Through use of a video camera to record the interference fringes dynamic processes may be studied with a time resolution of 20 ms. The method thus allows the dimensions of a single pore to be controlled continuously and reversibly, while monitoring the phase behaviour of matter confined to the pore. Material in the pore is in equilibrium with a bulk reservoir at the same temperature and pressure, so that any changes in the phase state from that of bulk are due solely to the influence of the pore walls.

If one of the surfaces is mounted so as to allow lateral movement along one of the cylinder axes the SFA may also be used to detect any response to lateral or shearing movements. It is thus possible to measure frictional forces between surfaces separated by very thin films, either through use of mechanical springs with strain gauges [161] or piezoelectric bimorphs [162].

Two types of experiment with the SFA have yielded experimental results of relevance for freezing and melting behaviour in confinement. First, small amounts of material may be condensed between the surfaces from vapour, and studied either as an annulus around the flattened surfaces in contact, or as a cylindrical bridge joining the separated surfaces (diameter, typically 10 μm and length, 5 nm–5 μm—see figure 14). This 'pore' has a single, well defined liquid–vapour interface, ensuring equilibrium at any temperature with little possibility of pore blockage. The large radius of curvature R of the surfaces ($R \sim 2$ cm) and the range over

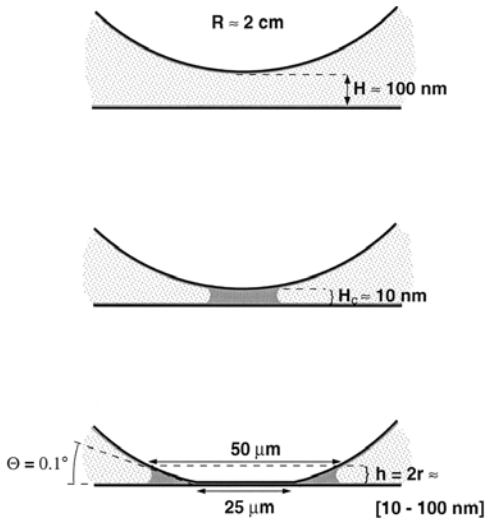

Figure 14. Cross-section of surfaces in the SFA in the equivalent sphere-on-a-flat configuration. The top shows non-interacting surfaces in vapour with adsorbed films. The middle shows the capillary-condensation transition at small separations (H_c). The bottom depicts the flattened surfaces in contact (separated by a thin film of liquid) and a condensate of size h ($= 2r$, where $r =$ radius of curvature of the condensate–vapour interface) in the annular wedge surrounding the contact zone. Note the relative magnitudes of lateral distances compared to normal separations.

which the separation H may be conveniently controlled and measured ($0 < H < 1000$ nm) mean that the dimensions of this pore are very different in directions parallel to the surfaces and normal to the surfaces. For finite surface separations the pore is effectively a thin film of thickness H, with the surfaces in contact the geometry becomes one of an annular wedge with a very small wedge angle—see figure 14, bottom.

Many of the most obvious properties of the confined material may be ascertained by direct light-microscopy observation. The large lateral distances allow optical detection of conditions in the pore despite the thin films involved—both with mutiple-beam interferometry and visible light microscopy (see figures 13 and 14).

Secondly, either with this condensed material or with bulk liquid introduced into the measuring chamber, the thin film (of thickness 0–5 nm and lateral extent 10–50 μm) between the flattened mica surfaces may be investigated. This is the method that has been used to measure forces across thin liquid films, and more recently study the behaviour of films when the surfaces are sheared against each other.

9.2. Capillary-condensation experiments

There is a large body of published work dealing with applications of the SFA to the study of capillary condensation from undersaturated vapour [163–170]. Verification of the Kelvin equation for capillary-condensed liquid of interfacial curvature down to 4 nm [163] was carried out with the SFA, as were the first systematic experiments on capillary condensation of a solute from solution [171–173] and measurements of the growth rate of capillary condensates [169, 174]. A current series of investigations is focussing on studies of capillary condensation of materials below their bulk melting points [160, 175–179] and these experiments are showing the potential of the SFA for carrying out controlled studies of freezing and melting phenomena in confinement.

A typical capillary-condensation experiment involves bringing the surfaces together in vapour. One surface is mounted on a rigid support with an effective spring constant of $\sim 10^5$ N m^{-1}. At a small separation—typically 10–15 nm—capillary condensation takes place and (despite the rigidity of the support) the surfaces are pulled into contact by the negative Laplace pressure in the connecting bridge that suddenly forms (see figure 14). The separation at which capillary condensation takes place in vapours of *tert*-butanol [166] and *n*-pentane [168] has been shown to be in agreement with a model based on the thickening of adsorbed films due to van der Waals forces between the opposing surfaces [180–182], at least for film thicknesses $t = 5$ nm. This separation as a function of relative vapour pressure (chemical potential) effectively gives the spinodal of the vapour–liquid transition in the slit.

If the surfaces are left in contact at $T > T_m$ the condensate grows to an equilibrium size determined by the Kelvin equation. On separation of the surfaces the annular condensate becomes a bridging neck, and the liquid in this bridge will evaporate at a separation determined by the Kelvin equation [163]. Modifications to the classical Kelvin equation due to the presence of adsorbed films of thickness t mean that a correction equal to $3t$ (in the case of complete wetting) has to be added to the surface separation H at which there is equilibrium between vapour and liquid [9, 183] (see section 2.1 and equations (2) and (4)). In practice this correction is usually within the bounds of experimental error. The size of the condensates is thus related to the contact angle of the liquid on the substrate and the surface separation at the location of the liquid–vapour interface, readily determined from the interference fringes. The hysteresis in the separation at which the bridge forms and evaporates is due solely to the first-order nature of the capillary-condensation transition. Close to coexistence this hysteresis is substantial—a condensate that forms on approach at a surface separation of 20 nm may only evaporate when the surfaces are 2000 nm apart.

The adhesion between two surfaces (of radius R) with a bridging condensate of radius of curvature r ($r \ll R$) is given by the sum of a Laplace-pressure contribution from the curved liquid–vapour interface with surface energy γ_{sl} and a direct solid–solid interaction F_{s-s} across the liquid in the condensate [104, 165],

$$F = 4\pi R\gamma_{sl} + F_{s-s}. \tag{13}$$

For simple liquids the capillary adhesion is essentially modulated by a solvation force like that measured in bulk liquids. This has been used to obtain information on solvation forces and adhesion forces in liquids by studying the interaction of surfaces in near-saturated vapour [165].

9.3. Liquid condensates below the melting point

If the typical capillary-condensation experiment is carried out below the bulk T_m the overall features are unaltered. There is no qualitative change in behaviour at T_m, although any change in wetting behaviour and the thickness of adsorbed films occurring in the vicinity of the melting point will quantitatively effect the capillary-condensation separation. A triple-point wetting transition occurring on isolated mica surfaces in *tert*-butanol vapour leads to a dramatic increase in the capillary-condensation separation at the melting point [177]—see figure 15. With some vapours, e.g. long-chain *n*-alkanes [174, 179], in the absence of an experimentally identifiable wetting transition, this separation does not change in the vicinity of T_m. This suggests that there is no obvious difference in the properties of adsorbed films above and below T_m of the bulk substance.

Capillary condensation as observed in the surface force apparatus is a fast process—the condensate forms and the surfaces are rapidly pulled into contact faster than the time resolution

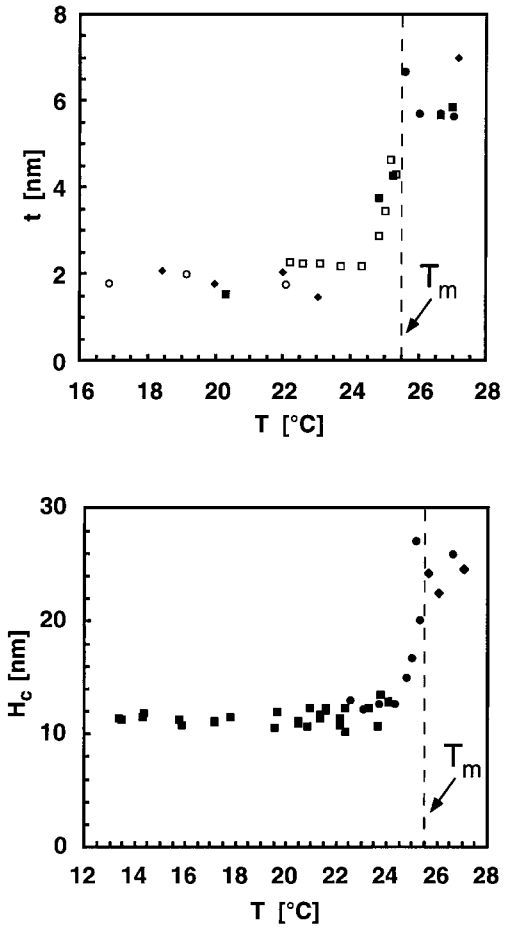

Figure 15. Measured film thickness t of *tert*-butanol adsorbed on an isolated mica surface as a function of temperature (top). Condensation separation H_c (at which the mica slit fills with liquid *tert*-butanol) for two mica surfaces across *tert*-butanol vapour as a function of temperature (bottom). In both graphs the vapour pressure is close to coexistence ($p/p_0 \sim 0.9996$ or higher, as determined for $T > T_m = 25.5\,^{\circ}$C—indicated by the dashed line). The different symbols are the results of separate experiments (Qiao Y and Christenson H K 1999 *Phys. Rev. Lett.* **83** 1371, copyright 1999 by the American Physical Society, used with permission).

of a standard video camera—20 ms. It is only after the annular wedge configuration has been attained that it is possible to study the condensate in more detail, usually by separation of the surfaces to ascertain whether or not the condensate flows, or to measure its refractive index. With one or two exceptions, discussed further below, the capillary condensates are clearly liquid—in some cases down to temperatures of 40 degrees below T_m.

The liquid in the condensates behaves in all respects as bulk liquid. Its refractive index is that of bulk, it flows readily, and the interaction between the surfaces across the liquid bridge is the same as that found between surfaces immersed in bulk liquid. As the surfaces are pushed together one may thus observe how the confined liquid is squeezed out, layer by layer, as successive barriers in the solvation interaction are surmounted (see section 9.7).

So far, the experiments have only probed conditions at or close to coexistence, i.e. when the material in the reservoir is either bulk solid or supercooled liquid. A slight heating effect

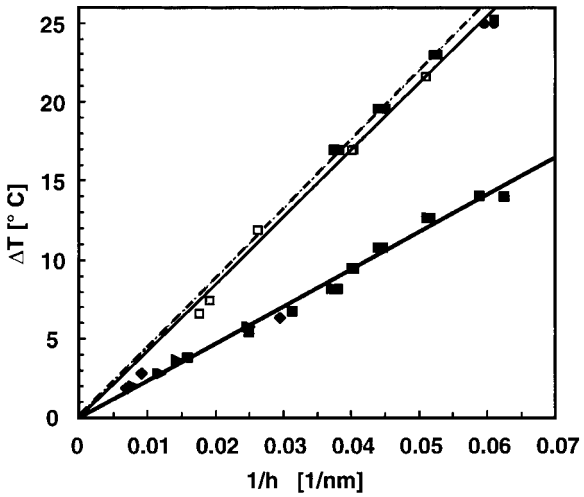

Figure 16. Temperature ΔT below the bulk melting point T_m as a function of the inverse equilibrium condensate size $1/h$ for *tert*-butanol (full squares, full line) *neo*-pentanol (full squares, dashed line) and menthol (unfilled squares, full line). The relative vapour pressure as determined from the condensate size at T_m was close to 1.00. From the slope of the lines the solid–liquid interfacial free energy may be determined from equation (14), with the results 13, 14 and 24 mJ m^{-2} for *tert*-butanol, *neo*-pentanol and menthol, respectively [175, 178].

due to the light beam that passes through the surfaces means that the relative vapour pressure at the surfaces is usually 0.995–0.998.

The difference compared to temperatures above T_m, where the condensate would of course grow almost indefinitely close to saturation, is that the size of the liquid condensates is limited. The lower the temperature, the smaller the equilibrium size, and a plot of ΔT against $1/h$ is linear (see figure 16). The flattened sphere-on-a-flat geometry leads to a theoretical relationship involving h (see figure 14, bottom), or [175, 160]

$$\Delta T = \frac{4V_m T_m[\gamma_{si} - \gamma_{li}]}{h\Delta H_f} = \frac{4V_m T_m \gamma_{sl}}{h\Delta H_f}. \tag{14}$$

This has been quantitatively studied for *tert*-butanol, *neo*-pentanol and menthol [175, 178], but the very low vapour pressure of some liquids (i.e. the longer-chain alkanes) leads to difficulties in achieving the equilibrium size. By simply measuring the size of capillary condensates formed from vapour in equilibrium with the bulk solid, one thus obtains the maximum size of a liquid condensate at a particular temperature, and this gives a measurement of the solid–liquid interfacial energy (subject to the usual assumptions) without the presence of any liquid–solid interface in the system.

If the temperature is lowered still further after the liquid condensate has reached its final size it will evaporate until equilibrium at the lower temperature has been reached. In no case has freezing of the liquid condensate been observed while the surfaces are still in contact. Condensation of solid can occur if nucleation from vapour takes place, either at the condensate–vapour interface or along the three-phase line at the mica surface. Condensation at isolated mica surfaces does not occur, the system is slightly off coexistence and it is never observed away from the contact zone.

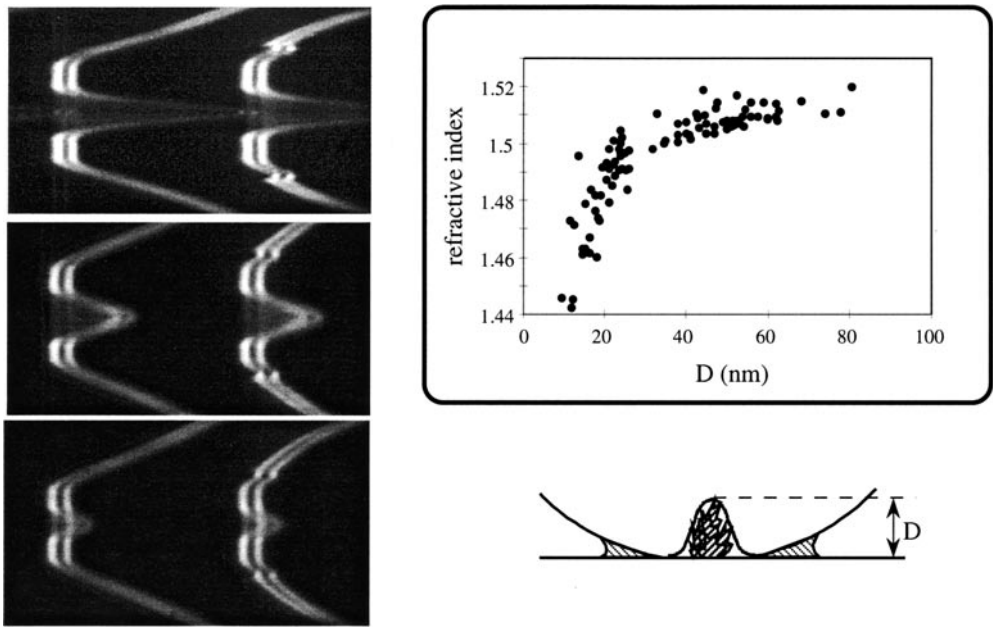

Figure 17. Interference fringes (left) and surface configuration deduced therefrom (lower right) for solid *n*-octadecane confined between two mica surfaces. The solid *n*-C_{18} is formed when a bridge of liquid *n*-C_{18} freezes on separation of the surfaces. As the surfaces are forced back into contact the mica deforms around the solid, and with time this remelts (sequence of fringes top to bottom). The refractive index of the confined solid decreases during the melting process and the surface separation (thickness of confined solid) decreases (top left). The refractive index of bulk liquid *n*-C_{18} is 1.44 and of solid *n*-C_{18} is 1.51–1.52 (reprinted from *Colloids and Surfaces* A **159** 135, copyright 1999, with permission from Elsevier Science).

9.4. Freezing of condensates

In some cases condensed liquid will freeze or crystallize when the surfaces are separated. This occurs for long-chain *n*-alkanes C_mH_{2m+2} ($m = 16$–18), and more readily the lower the temperature [176, 179]. Studies with *n*-octadecane have shown that a few degrees below T_m freezing occurs only after the liquid condensate has snapped by separating the surfaces a large distance [176]. As the temperature is lowered the condensate freezes while still connecting the two surfaces, and at still lower temperatures immediately upon separation from contact. If the surfaces are pushed together again, they can be made to deform and wrap around the solid, but after confinement has once again been achieved the solid will remelt—see figure 17. Condensates of tetradecane, on the other hand, do not freeze under these conditions down to 7 degrees below T_m [179].

This freezing and melting behaviour may be qualitatively rationalized by considering the relative areas of the alkane–mica and alkane–vapour interfaces. *n*-Alkanes with carbon numbers $m \geqslant 15$ show surface ordering (surface freezing) [184, 185], and bulk solid nucleates easily from the liquid–vapour interface. As the area of the liquid–vapour interface increases at the expense of the mica–liquid interface on separation from contact freezing occurs more readily. Tetradecane does not show surface ordering, and it behaves in this respect more like other liquids such as the alcohols, where freezing is inhibited at moderate temperature depressions.

If the temperature is lowered with a condensate of *n*-octadecane around the surfaces in contact, one may observe the growth of crystals from the condensate–vapour interface out into the vapour phase [176]. These observations are also consistent with the ability of the liquid–alkane surface to nucleate bulk crystals. The crystallites, however, tend not to grow into the liquid condensate. Similar experiments with *tert*-butanol lead to evaporation of the condensate, as discussed above [160, 175].

9.5. Nucleation of solid from vapour

In the case of tetrabromomethane the phase state of the initially condensed material is uncertain [186]. As soon as one can reverse the relative motion of the surfaces in order to attempt to separate them it is clear that they are being held together by solid–solid adhesion rather than a liquid condensate. Here, too it may be that the innermost part of the annular wedge around the contact zone is filled with liquid, and solid is only present outside this region. Further work is required to resolve this question.

Sufficiently far below T_m direct condensation of solid from vapour will undoubtedly occur under some circumstances. This is the case with *neo*-pentanol [175, 178] and perhaps dodecafluorocyclohexane [187], where accumulation of solid in the annular wedge, outside the liquid–vapour interface, can be observed. Solid is identified by the fact that the adhesion is an order of magnitude larger than with liquid condensates. The solid acts as an adhesive gluing the surfaces together and separation takes place via the breaking of solid–mica or solid–solid contact. A quantitative comparison with values expected from surface energies is not straightforward due to the lack of knowledge of the area of the rupture and the occurrence of substantial surface deformations. After separation the solid condensates sublime if the vapour pressure of the material is sufficiently high.

It appears likely that the solid forms by condensation of new material from the vapour phase outside an annulus of liquid, rather than by freezing of condensed liquid. The considerable differences in behaviour found between different substances are probably related to barriers for nucleation at the liquid–vapour interface, or at the adsorbed film–vapour interface. One may speculate that the relative ease of nucleation of solid in the case of *neo*-pentanol and dodecafluorocyclohexane is related to the structure of the disordered (plastic) bulk crystalline phases of both substances at these temperatures. Tetrabromomethane also has a plastic crystal as the stable phase at room temperature. Solid does not condense from menthol vapour at similar ΔT values, and the films of menthol adsorbed to mica do not show clear layering transitions. With *neo*-pentanol it appears that the properties of the solid condensate change with temperature, as shown by measurements of the refractive index, the rate of growth of the condensates, their apparent equilibrium size and their behaviour under applied loads [178]. We are only beginning to explore the possible applications of the SFA to the study of confined solids, and in particular their direct condensation or nucleation from vapour. Studies of the effects of the degree of crystallinity of the substrate would be particularly useful—porous materials are often amorphous in nature.

9.6. Condensates in equilibrium with supercooled liquid

If the experiment is carried out over supercooled liquid rather than solid the condensates at a given temperature are larger, as expected due to the higher vapour pressure. Otherwise, the properties of the condensate are similar. Quantitative measurements with *tert*-butanol have so far been unsuccessful due to condensation of solid at other points in the chamber, thus precluding true equilibrium in the vapour phase.

9.7. Experiments with thin films—force measurements

With the surfaces close to contact one may study the effect of confinement on the structure of the liquid, and measure the force between the surfaces. In most pure, non-aqueous liquids the short-range interaction is a solvation force, and this has been extensively studied above T_m [188, 189], even in capillary condensates [165]. The force as a function of separation oscillates between repulsive maxima and attractive minima, usually with a period close to the mean molecular diameter. The measurable range of the solvation force is up to about 10 molecular diameters with near-spherical molecules, while more asymmetric molecules show fewer oscillations. *n*-Alkanes layer parallel to the surfaces when confined and give rise to a force with a period close to the thickness of the alkyl chains ($\sim$0.4) [190]. Measurements with octamethylcyclotetrasiloxane, which is easily supercooled, have shown that the force is unchanged from 11 degrees above to 4 degrees below T_m [191].

When capillary condensation occurs below T_m the surfaces come together separated by a thin film of liquid, as in figure 14, bottom. The large adhesion due to the condensate leads to extensive surface flattening, and the result is a slit perhaps 50 μm in diameter but of a thickness of only nanometres. Qualitatively, the material in this slit behaves exactly as it does during force measurements with the bulk liquid above T_m at similar separations, where the extent of flattening is less. The repulsive barriers of the solvation force are evident on pushing the surfaces together, and in some cases the innermost adhesive minima may also be identified. Preliminary results have been obtained with *tert*-butanol, *neo*-pentanol and dodecafluorocyclohexane. With respect to application of normal loads the film between the confining surfaces remains liquid-like down to low temperatures. It may therefore appear surprising that a number of recent studies of the response of these films to lateral shearing of the surfaces have suggested transitions to solid-like behaviour *above* T_m.

9.8. Experiments with thin films—shear

If two flat surfaces, separated by a thin film of liquid, are made to slide against each other the response of the second surface to the motion of the first depends on the viscosity of the liquid. One measures a 'frictional force' that is proportional to the area of contact, the viscosity, the relative velocity of the surfaces and inversely proportional to the surface separation. Experiments with the SFA have shown that this behaviour breaks down in molecularly thin films, where the surfaces are separated by only a few layers of molecules. The results have generally been discussed in terms of transitions to solid-like or glasslike behaviour in these films, at temperatures above T_m of the liquids. In the solid-like state, a critical shear stress is required to initiate sliding.

During shear of mica surfaces separated by films of *n*-hexadecane, *n*-decane and octamethylcyclotetrasiloxane one to three molecular layers thick the transition between liquid-like and solid-like response was found (see figure 18) to depend on the applied load [162]. The change in behaviour was very sudden, but reversible. By contrast, a more gradual transition to solid-like dynamic behaviour and the great complexity of the response to shear in thin films was discussed by Gee *et al* [161]. It was subsequently reported that the transition in viscoelastic response during shearing of OMCTS films between mica surfaces was inconsistent with a freezing (first-order) transition; instead there was a smooth change to a slower relaxation and increased rigidity of the film [192].

The most recent work presents evidence for an abrupt, first-order transition to solid-like shear behaviour for OMCTS and cyclohexane films [193–195]. Moreover, in this study the transition was observed at a separation of six molecular diameters, under very low applied

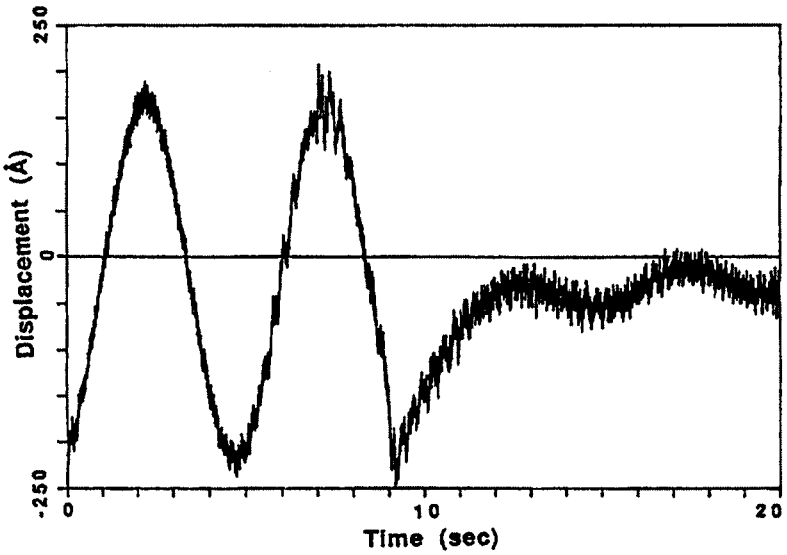

Figure 18. Oscillation amplitude as a function of time when two mica surfaces separated by two molecular layers of octamethylcyclotetrasiloxane (OMCTS) ($d = 1.8$ nm), under an (average) normal pressure of 3.6 MPa, are sheared against each other. The change in the amplitude–t curve at $t \sim 9$ s indicates that a sudden transition from liquid-like to solid-like behaviour of the OMCTS film has occurred (Van Alsten J and Granick S 1988 *Phys. Rev. Lett.* **61** 2570, copyright 1988 by the American Physical Society, used with permission).

loads. Recent reviews have discussed these experimental observations and their interpretation [196, 197].

There is thus an apparent contradiction between the results of the shearing experiments and those of the force measurements. In the former case, thin films of liquid show solid-like behaviour above the bulk melting point, whereas in the latter case films of the same or similar substances show a liquid-like response to normal loads below the bulk melting point.

It is uncertain whether or not a difference in time scale of the respective experiments is responsible. During a force measurement, the load on the surfaces is increased gradually or stepwise, but the movement of the surfaces is retarded to a considerable extent by film drainage from between the surfaces—the liquid has to be squeezed out from a very thin but laterally quite extended film (see dimensions in figure 14, bottom). (The pressure distribution across the thin film is not uniform but shows a maximum in the centre. This may well aid in the extrusion of liquid.) It is thus not possible to bring the surfaces together quickly. Indeed, observations have clearly shown that the time taken for each layer of molecules to be ejected from between the surfaces increases dramatically at small separations [172], and reaches the order of 0.1 s for the penultimate layer. Removal of the last layer can only take place after break-through has occurred between the parallel surfaces at some point across the monomolecular layer.

During the shearing experiments the surfaces are moved laterally by tens or hundreds of nanometres at frequencies of 1–500 Hz, depending on the instrumentation used. The maximum speeds involved are often, but not always, considerably greater than during force measurements. However, the molecules closest to each surface will be constrained to follow that surface, and if the hindered diffusion in the thin film cannot keep up with the lateral motion, the result may be a temporary 'freezing-in' of the liquid structure. It is perhaps significant that x-ray diffraction experiments with graphitic microfibres point to solid-like ordering of liquid in the films (of

comparable dimensions, but with different substrate surfaces) at temperatures far above their bulk melting point [147, 148, 151].

10. Summary

Most experimental results may be divided into two groups—one with larger pore sizes ($d \geqslant 3$–4 nm) where it seems that the behaviour can essentially be understood in terms of pockets of 'bulk' substance surrounded by independent interfaces, and a second group ($d \leqslant 3$–4 nm) where no part of the system shows anything approaching bulk behaviour and the interfaces are not independent. In the first category the melting and freezing points are depressed compared to bulk, with the typical linear ΔT against $1/r$ behaviour (often also found for solid–solid transitions), usually with a liquid-like layer next to the pore walls. For the smaller pore sizes in this group the enthalpy of fusion is reduced compared to bulk, and below the melting point the system may often be modelled as a frozen core with a liquid-like layer next to the pore wall. This type of behaviour is found with the porous glasses of $d > 3$–4 nm, with MCM-41 of larger pore size, and with the capillary condensates in the SFA, and may be termed 'classical capillary-melting behaviour'.

The second category consists of the porous glasses with the smallest pores as well as most of the MCM-41 (and similar materials) and graphitic microfibre systems described here. Because the interfaces are close together, division into surface and 'bulk' is no longer possible. Indeed, the structure of the confined material, above and below the bulk T_m is qualitatively different from bulk, and phase transitions are smeared (as expected from finite-size effects) or vanish altogether.

There would appear to be rather clear differences in freezing and melting behaviour between that found with the porous glasses and that found in the cylindrical pores of MCM-41. One difference is obviously related to the pore-size uniformity and lack of interconnectivity, giving less hysteresis with MCM-41. In MCM-41 the behaviour is often qualitatively different from that in bulk. The very narrow slit-pores of graphitic microfibres (ACF) show even greater deviations in behaviour of the confined fluids. In these films of two or three molecular layers the usual 3D melting and freezing transitions are absent, and properties such as molecular mobilities are intermediate between those found in bulk solid and in bulk liquid.

It is tempting to compare this break-down of bulk behaviour with the conclusions drawn from the results of shearing experiments with the SFA. The film thicknesses involved are similar, and perhaps the transition to 'solid-like behaviour' is best viewed as a consequence of a gradual cross-over to 2D behaviour in thin films. The results of shearing experiments on the one hand and of force measurements on the other point to differences between dynamic and static properties in these systems, especially when bulk concepts are used to interpret the results.

The SFA is clearly capable of providing a different and complementary approach to the study of freezing and melting in confinement. The unhindered contact with the vapour phase and the wedge shape of the single pore ensures that bulk solid, capillary-condensed liquid and vapour are in equilibrium. In particular, the SFA allows the study of both direct nucleation from vapour as well as freezing of condensed liquid.

Acknowledgments

I am grateful to R Evans for helpful comments and discussions, and to Lloyd for taking such delight in his own confinement.

References

[1] Thomson W 1871 *Phil. Mag.* (IV) **42** 448
[2] Evans R and Marini Bettolo Marconi U 1987 *J. Chem. Phys.* **86** 7138
[3] Evans R 1990 *J. Phys.: Condens. Matter* **2** 8989
[4] Batchelor R W and Foster A G 1944 *Trans. Faraday Soc.* **40** 300
[5] Defay R, Prigogine I, Bellemans A and Everett D H 1966 *Surface Tension and Adsorption* (London: Longmans)
[6] Reiss H and Wilson I B 1948 *Colloid Science* **3** 551
[7] Brun M, Lallemand A, Quinson J F and Eyraud C 1973 *J. Chim. Phys.* **70** 979
[8] Brun M, Lallemand A, Quinson J-F and Eyraud C 1977 *Thermochim. Acta* **21** 59
[9] Derjaguin B V 1940 *Acta Physicochim. URSS* **12** 181
[10] See, for example, proceedings of the International Workshop on Dynamics in Confined Systems 2000 *J. Physique.* IV **10** Pr7
[11] Peppiatt S J and Sambles J R 1975 *Proc. R. Soc.* A **345** 387
[12] Peppiatt S J and Sambles J R 1975 *Proc. R. Soc.* A **345** 401
[13] Couchman P R and Jesser W A 1977 *Nature* **269** 481
[14] Johari G P, Pascheto W and Jones S J 1994 *J. Chem. Phys.* **100** 4548
[15] Salvetti G, Tombari E and Johari G P 1995 *J. Chem. Phys.* **102** 4987
[16] Weiss J A, Oxtoby D W, Grier D G and Murray C A 1995 *J. Chem. Phys.* **103** 1180
[17] Loewen H, Watzlawek M, Likos C N, Schmidt M, Jusufi A and Denton A R 2000 *J. Phys.: Condens. Matter* **12** A465
[18] Navascues G and Tarazona P 1987 *Mol. Phys.* **62** 497
[19] Diestler D J, Schoen M and Cushman J H 1993 *Science* **262** 545
[20] Schoen M, Cushman J H and Diestler D J 1993 *Mol. Phys.* **81** 475
[21] Curry J E, Zhang F, Cushman J H, Schoen M and Diestler D J 1994 *J. Chem. Phys.* **101** 10 824
[22] Koga K, Zeng X C and Tanaka H 1997 *Phys. Rev. Lett.* **79** 5262
[23] Maddox M W and Gubbins K E 1997 *J. Chem. Phys.* **107** 9659
[24] Miyahara M and Gubbins K E 1997 *J. Chem. Phys.* **106** 2865
[25] Slovak J, Koga K, Tanaka H and Zeng X C 1997 *Phys. Rev.* E **60** 5833
[26] Gao J, Luedtke W D and Landman U 1997 *Phys. Rev. Lett.* **79** 705
[27] Sliwinska-Bartkowiak M, Gras J, Sikorski R, Radhakrishnan R, Gelb L and Gubbins K E 1999 *Langmuir* **15** 6060
[28] Dominguez H, Allen M P and Evans R 1999 *Mol. Phys.* **96** 209
[29] Miyahara M, Kanda H, Shibao M and Higashitani K 2000 *J. Chem. Phys.* **112** 9909
[30] Radhakrishnan R, Gubbins K E and Sliwinska-Bartkowiak M 2000 *J. Chem. Phys.* **112** 11 048
[31] Gubbins K E, Sliwinska-Bartkowiak M and Suh S-H 1996 *Mol. Simul.* **17** 333
[32] Gelb L D, Gubbins K E, Radhakrishnan R and Sliwinska-Bartkowiak M 1999 *Rep. Prog. Phys.* **62** 1573
[33] Foote H W and Saxton B J 1916 *J. Am. Chem. Soc.* **38** 588
[34] Foote H W and Saxton B 1917 *J. Am. Chem. Soc.* **39** 1103
[35] Coolidge A S J 1924 *J. Am. Chem. Soc.* **46** 596
[36] Jones I D and Gortner R A 1932 *J. Phys. Chem.* **36** 387
[37] Patrick W A and Land W E 1934 *J. Phys. Chem.* **38** 1201
[38] Milligan W O and Rachford H 1948 *J. Am. Chem. Soc.* **70** 2922
[39] Brown M J and Foster A G 1952 *Nature* **169** 37
[40] Patrick W A and Kemper W A 1938 *J. Phys. Chem.* **42** 369
[41] Higuti I and Yoshimoto I 1952 *J. Phys. Chem.* **56** 921
[42] Puri B R, Sharma L R and Lakhanpal M L 1954 *J. Phys. Chem.* **58** 289
[43] Berezin G I, Kiselev A V and Kozlov A A 1973 *J. Colloid Interface Sci.* **45** 190
[44] Pearson R T and Derbyshire W 1974 *J. Colloid Interface Sci.* **46** 232
[45] Hall P G, Williams R T and Slade R C T 1985 *J. Chem. Soc. Faraday Trans.* I **81** 847
[46] Drake J M and Klafter J 1990 *Phys. Today* **43** 46
[47] Levitz P, Ehret G, Sinha S K and Drake J M 1991 *J. Chem. Phys.* **95** 6151
[48] Mitropoulos A C, Haynes J M, Richardson R M and Kanellopoulos N K 1995 *Phys. Rev.* B **52** 10 035
[49] Hodgson C and McIntosh R 1959 *Can. J. Chem.* **37** 1278
[50] Hodgson C and McIntosh R 1960 *Can. J. Chem.* **38** 958
[51] Litvan G and McIntosh R 1963 *Can. J. Chem.* **41** 3095
[52] Litvan G G 1966 *Can. J. Chem.* **44** 2617
[53] Rennie G K and Clifford J 1977 *J. Chem. Soc. Faraday Trans.* I **73** 680
[54] Enüstün B V, Sentürk H S and Yurdakul O 1978 *J. Colloid Interface Sci.* **65** 509

[55] Jones D R H 1974 *J. Mater. Sci.* **9** 1
[56] Ginzburg V L and Sobyanin N 1972 *Sov. Phys.–JETP Lett.* **15** 242
[57] Maris H J, Seidel G M, and Huber T E 1983 *J. Low Temp. Phys.* **51** 471
[58] Thomson A L, Brewer D F, Naji T, Haynes S and Reppy J D 1981 *Physica* B **107** 581
[59] Brewer D F, Liezhao C, Girit C and Reppy J D 1981 *Physica* B **107** 583
[60] Smith E N, Brewer D F, Liezhao C and Reppy J D 1981 *Physica* B **107** 585
[61] Beamish J R, Hikata A, Tell L and Elbaum C 1983 *Phys. Rev. Lett.* **50** 425
[62] Adams E D, Tang Y H, Uhlig K and Haas G E 1987 *J. Low Temp. Phys.* **66** 85
[63] Beamish J R, Mulders N, Hikata A and Elbaum C 1991 *Phys. Rev.* B **44** 9314
[64] Bittner D N and Adams E D 1994 *J. Low Temp. Phys.* **97** 519
[65] Molz E B and Beamish J R 1995 *J. Low Temp. Phys.* **101** 1055
[66] Finotello D, Gillis K A, Wong A and Chan M H W 1988 *Phys. Rev. Lett.* **61** 1954
[67] Golov A and Pobell F 1995 *J. Low Temp. Phys.* **101** 373
[68] Tell J L and Maris H J 1983 *Phys. Rev.* B **28** 5122
[69] Torii R H, Maris H J and Seidel G M 1990 *Phys. Rev.* B **41** 7167
[70] Grebener S, Sartakov B, Toennies J P and Vilesov A F 2000 *Science* **289** 1532
[71] Sokol P E, Ma W J, Herwig K W, Snow W M, Wang Y, Koplik J and Banavar J R 1992 *Appl. Phys. Lett.* **61** 777
[72] Wang Y, Snow W M and Sokol P E 1995 *J. Low Temp. Phys.* **101** 929
[73] Sokol P E, Azuah R T, Gibbs M R and Bennington S M 1996 *J. Low Temp. Phys.* **103** 23
[74] Kondo Y, Schindler M and Pobell F 1995 *J. Low Temp. Phys.* **101** 195
[75] Schindler M, Dertinger A, Kondo Y and Pobell F 1996 *Phys. Rev.* B **53** 11 451
[76] Molz E, Wong A P Y, Chan M H W and Beamish J R 1993 *Phys. Rev.* B **48** 5741
[77] Schäfer B, Balszunat D, Langel W and Asmussen B 1996 *Mol. Phys.* **89** 1057
[78] Brown D W, Sokol P E and Ehrlich S N 1998 *Phys. Rev. Lett.* **81** 1019
[79] Huber P and Knorr K 1999 *Phys. Rev.* B **60** 12 657
[80] Warnock J, Awschalom D D and Shafer M W 1986 *Phys. Rev. Lett.* **57** 1753
[81] Awschalom D D and Warnock J 1987 *Phys. Rev.* B **35** 6779
[82] Schirato B S, Fang M P, Sokol P E and Komarneni S 1995 *Science* **267** 369
[83] Huber P, Wallacher D and Knorr K 1998 *J. Low Temp. Phys.* **111** 419
[84] Huber P, Wallacher D and Knorr K 1999 *Phys. Rev.* B **60** 12 666
[85] Duffy J A, Wilkinson N J, Fretwell H M, Alam M A and Evans R 1995 *J. Phys.: Condens. Matter* **7** L713
[86] Fretwell H M, Duffy J A, Clarke A P, Alam M A and Evans R 1996 *J. Phys.: Condens. Matter* **8** 9613
[87] Alam M A, Fretwell H M, Duffy J A, Clarke A P and Dugdale S B 1996 *J. Radioanal. Nucl. Chem.* **210** 255
[88] Duffy J A, Fretwell H M, Clarke A P, Dugdale S B and Alam M A 1996 *J. Radioanal. Nucl. Chem.* **211** 173
[89] Duffy J A, Wilkinson N J, Fretwell H M and Alam M A 1995 *J. Phys.: Condens. Matter* **7** L27
[90] Duffy J A and Alam M A 2000 *Langmuir* **16** 9513
[91] Brown D W, Sokol P E, Clarke A P, Alam M A and Nuttall W J 1997 *J. Phys.: Condens. Matter* **9** 7317
[92] Balszunat D, Asmussen B, Müller M, Press W, Langel W, Coddens G, Ferrand M and Büttner H 1996 *Physica* B **226** 185
[93] Gutt C, Asmussen B, Krasnov I, Press W, Langel W and Kahn R 1999 *Phys. Rev.* B **59** 8607
[94] Krasnov I A, Asmussen B, Gutt C, Press W, Langel W and Ferrand M 2000 *J. Phys.: Condens. Matter* **12** 1613
[95] Dore J C, Dunn M, Hasebe T and Strange J H 1989 *Colloids Surf.* **36** 199
[96] Jackson C L and McKenna G B 1990 *J. Chem. Phys.* **93** 9002
[97] Mu R and Malhotra V M 1991 *Phys. Rev.* B **44** 4296
[98] Strange J H, Rahman M and Smith E G 1993 *Phys. Rev. Lett.* **71** 3589
[99] Hansen E W, Schmidt R and Stöcker M 1996 *J. Phys. C: Solid State Phys.* **100** 11 396
[100] Booth H F and Strange J H 1998 *Mol. Phys.* **93** 263
[101] Aksnes D W and Gjerdaker L 1999 *J. Mol. Struct.* **475** 27
[102] Mu R, Xue Y, Henderson D O and Frazier D O 1996 *Phys. Rev.* B **53** 6041
[103] Grosse K, Ratke L and Feuerbacher B 1997 *Phys. Rev.* B **55** 2894
[104] Fisher L R and Israelachvili J N 1981 *Colloids Surf.* **3** 303
[105] Takei T, Onoda Y, Fuji M, Watanabe T and Chikazawa M 2000 *Thermochim. Acta* **352–353** 199
[106] Steytler D C, Dore J C and Wright C J 1983 *J. Phys. Chem.* **87** 2458
[107] Steytler D C and Dore J C 1985 *Mol. Phys.* **56** 1001
[108] Baker J M, Dore J C and Behrens P 1997 *J. Phys. Chem.* B **101** 6226
[109] Overloop K and Van Gerven L 1993 *J. Magn. Reson.* A **101** 179
[110] Bellissent-Funel M-C, Lal J and Bosio L 1993 *J. Chem. Phys.* **98** 4246
[111] Hirama Y, Takahashi T, Hino M and Sato T 1996 *J. Colloid Interface Sci.* **184** 349

[112] Takamuku T, Yamagami M, Wakita H, Masuda Y and Yamaguchi T 1997 *J. Phys. Chem.* B **101** 5730
[113] Ramsay J D F and Poinsignon C 1987 *Langmuir* **3** 320
[114] Chen S-H, Bellissent-Funel M-C and Zanotti J-M 1995 *Phys. Rev.* E **51** 4558
[115] Zanotti J-M, Bellissent-Funel M-C and Chen S-H 1999 *Phys. Rev.* E **59** 3084
[116] Ramsay J D F 1998 *Adv. Colloid Interface Sci.* **76/77** 13
[117] Unruh K M, Huber T E and Huber C A 1993 *Phys. Rev.* B **48** 9021
[118] Kumzerov Yu A, Nabereznon A A, Vakrushev S B and Savenko B N 1995 *Phys. Rev.* B **52** 4772
[119] Borisov B F, Charnaya E V, Plotnikov P G, Hoffman W-D, Michel D, Kumzerov Yu A, Tien C and Wur C-S 1998 *Phys. Rev.* B **58** 5329
[120] Michel D, Borisov B F, Charnaya E V, Hoffmann W-D, Plotnikov P G and Kumzerov Yu A 1999 *Nanostruct. Mater.* **12** 515
[121] Tien C, Wur C S, Lin K J, Hwang J S, Charnaya E V and Kumzerov Yu A 1996 *Phys. Rev.* B **54** 11 880
[122] Borisov B F, Charnaya E V, Hoffman W D, Michel D, Shelyapin A V and Kumzerov Yu A 1997 *J. Phys.: Condens. Matter* **9** 3377
[123] Charnaya E V, Tien C, Lin K J and Kumzerov Yu A 1998 *Phys. Rev.* B **58** 11089
[124] Beale M I J, Chew N G, Uren M J, Cullis A G and Benjamin J D 1985 *Appl. Phys. Lett.* **46** 86
[125] Faivre C, Bellet D and Dolino G 1999 *Eur. Phys. J.* B **7** 19
[126] Kresge C T, Leonowicz M E, Roth W J, Vartuli J C and Beck J S 1992 *Nature* **359** 710
[127] Beck J S, Vartuli J C, Roth W J, Leonowicz M E, Kresge C T, Schmitt K D, Chu C T-W, Olson D H, Sheppard E W, McCullen S B, Higgins J B and Schlenker J L 1992 *J. Am. Chem. Soc.* **114** 10 834
[128] Zhao D, Huo Q, Feng J, Chmelka B F and Stucky G D 1998 *J. Am. Chem. Soc.* **120** 6024
[129] Inagaki S, Fukushima Y and Kuroda K 1993 *Chem. Commun.* **680**
[130] Llewellyn P L, Grillet Y, Rouquerol J, Martin C and Coulomb J-P 1996 *Surf. Sci.* **352–354** 468
[131] Akporiaye D, Hansen E W, Schmidt R and Stöcker M 1994 *J. Phys. Chem.* **98** 1926
[132] Hansen E W, Schmidt R, Stöcker M and Akporiaye D 1995 *J. Phys. Chem.* **99** 4148
[133] Schmidt R, Hansen E W, Stöcker M, Akporiaye D and Ellestad O H 1995 *J. Am. Chem. Soc.* **117** 4049
[134] Morishige K and Nobuoka K 1997 *J. Chem. Phys.* **107** 6965
[135] Morishige K and Shikimi M 1998 *J. Chem. Phys.* **108** 7821
[136] Morishige K and Kawano K 1999 *J. Chem. Phys.* **110** 4867
[137] Edler K J, Reynolds P A, Trouw F and White J W 1996 *Chem. Phys. Lett.* **249** 438
[138] Morishige K and Kawano K 1999 *J. Phys. Chem.* B **103** 7906
[139] Morineau D, Dosseh G, Alba-Simionesco C and Llewellyn P 1999 *Phil. Mag.* B **79** 1847
[140] Dosseh G, Morineau D and Alba-Simionesco C 2000 *J. Physique.* IV **10** Pr7-99
[141] Morishige K and Kawano K 2000 *J. Phys. Chem.* B **104** 2894
[142] Morishige K, Kawano K and Hayashagi T 2000 *J. Phys. Chem.* B **104** 10 298
[143] Morishige K and Kawano K 2000 *J. Chem. Phys.* **112** 11 023
[144] Morishige K and Kawano K 2000 *J. Physique.* IV **10** Pr7-91
[145] Suzuki M 1994 *Carbon* **32** 577
[146] Kaneko K, Ishii C, Ruike M and Kuwabara H 1992 *Carbon* **30** 1075
[147] Iiyama T, Nishikawa N, Suzuki T and Kaneko K 1997 *Chem. Phys. Lett.* **274** 152
[148] Iiyama T, Nishikawa N, Suzuki T, Otowa T, Hijiriyama M, Nojima Y and Kaneko K 1999 *J. Phys. Chem.* B **101** 3037
[149] Kaneko K, Watanabe A, Iiyama T, Radhakrishnan R and Gubbins K E 1999 *J. Phys. Chem.* B **103** 7061
[150] Watanabe A, Iiyama T and Kaneko K 1999 *Chem. Phys. Lett.* **305** 71
[151] Ohkubo T, Iiyama T, Nishikawa N, Suzuki T and Kaneko K 1999 *J. Phys. Chem.* B **103** 1859
[152] Meissner F 1920 *Z. Anorg. Allg. Chem.* **110** 169
[153] Sill R C and Skapski A S 1956 *J. Chem. Phys.* **24** 644
[154] Skapski A, Billups R and Rooney A 1957 *J. Chem. Phys.* **25** 1350
[155] Skapski A, Billups R and Casavant D 1959 *J. Chem. Phys.* **31** 1431
[156] Israelachvili J N and Adams G E 1978 *J. Chem. Soc. Faraday Trans.* I **74** 975
[157] Klein J 1983 *J. Chem. Soc. Faraday Trans.* I **79** 99
[158] Parker J L, Christenson H K and Ninham B W 1989 *Rev. Sci. Instrum.* **60** 3135
[159] Israelachvili J N 1973 *J. Colloid Interface Sci.* **44** 259
[160] Christenson H K 1997 *Colloids Surf.* **123** 355.
[161] Gee M L, McGuiggan P M, Israelachvili J N and Homola A M 1990 *J. Chem. Phys.* **93** 1895
[162] Van Alsten J and Granick S 1988 *Phys. Rev. Lett.* **61** 2570
[163] Fisher L R and Israelachvili J N 1981 *J. Colloid Interface Sci.* **80** 528
[164] Christenson H K 1988 *J. Colloid Interface Sci.* **121** 170
[165] Christenson H K and Yaminsky V V 1993 *Langmuir* **9** 2448

[166] Christenson H K 1994 *Phys. Rev. Lett.* **73** 1821
[167] Wanless E J and Christenson H K 1994 *J. Chem. Phys.* **101** 4260
[168] Curry J E and Christenson H K 1996 *Langmuir* **12** 5729
[169] Kohonen M M, Maeda N and Christenson H K 1999 *Phys. Rev. Lett.* **82** 4667
[170] Kohonen M M and Christenson H K 2000 *Langmuir* **16** 7285
[171] Christenson H K 1985 *J. Colloid Interface Sci.* **104** 234
[172] Christenson H K and Blom C E 1987 *J. Chem. Phys.* **86** 419
[173] Christenson H K, Fang J and Israelachvili J N 1989 *Phys. Rev.* B **39** 11 750
[174] Maeda N, Kohonen M M and Christenson H K 1999 *Phys. Rev.* E **61** 7239
[175] Christenson H K 1995 *Phys. Rev. Lett.* **74** 4675
[176] Maeda N and Christenson H K 1999 *Colloids Surf.* A **159** 135
[177] Qiao Y and Christenson H K 1999 *Phys. Rev. Lett.* **83** 1371
[178] Qiao Y and Christenson H K 2001 *Phys. Rev. Lett.* at press
[179] Maeda N, Kohonen M M and Christenson H K *J. Phys. Chem.* at press
[180] Derjaguin B V and Churaev N V 1976 *J. Colloid Interface Sci.* **54** 157
[181] Forcada M L 1993 *J. Chem. Phys.* **98** 639
[182] Iwamatsu M and Horii K 1996 *J. Colloid Interface Sci.* **182** 400
[183] Evans R and Marini Bettolo Marconi U 1985 *Chem. Phys. Lett.* **114** 415
[184] Earnshaw J C and Hughes C J 1992 *Phys. Rev.* A **46** 4494
[185] Ocko B M, Wu X Z, Sirota E B, Sinha S K, Gang O and Deutsch M 1997 *Phys. Rev.* E **55** 3164
[186] Christenson H K unpublished observations
[187] Maeda N and Christenson H K in preparation
[188] Christenson H K 1988 *J. Dispersion Sci. Technol.* **9** 171
[189] Israelachvili J N 1991 *Intermolecular and Surface Forces* 2nd edn (New York: Academic)
[190] Christenson H K, Gruen D W R, Horn R G and Israelachvili J N 1987 *J. Chem. Phys.* **87** 1834
[191] Christenson H K and Israelachvili J N 1984 *J. Chem. Phys.* **80** 4566
[192] Demirel A L and Granick S 1996 *Phys. Rev. Lett.* **77** 2261
[193] Klein J and Kumacheva E 1995 *Science* **269** 816
[194] Klein J and Kumacheva E 1998 *J. Chem. Phys.* **108** 6996
[195] Kumacheva E and Klein J 1998 *J. Chem. Phys.* **108** 7010
[196] Kumacheva E 1998 *Prog. Surf. Sci.* **58** 75
[197] Hu Y-Z and Granick S 1998 *Tribol. Lett.* **5** 81–8